Molecular Cell

Resource

Ubiquitin-independent proteasomal degradation driven by C-degron pathways

Graphical abstract

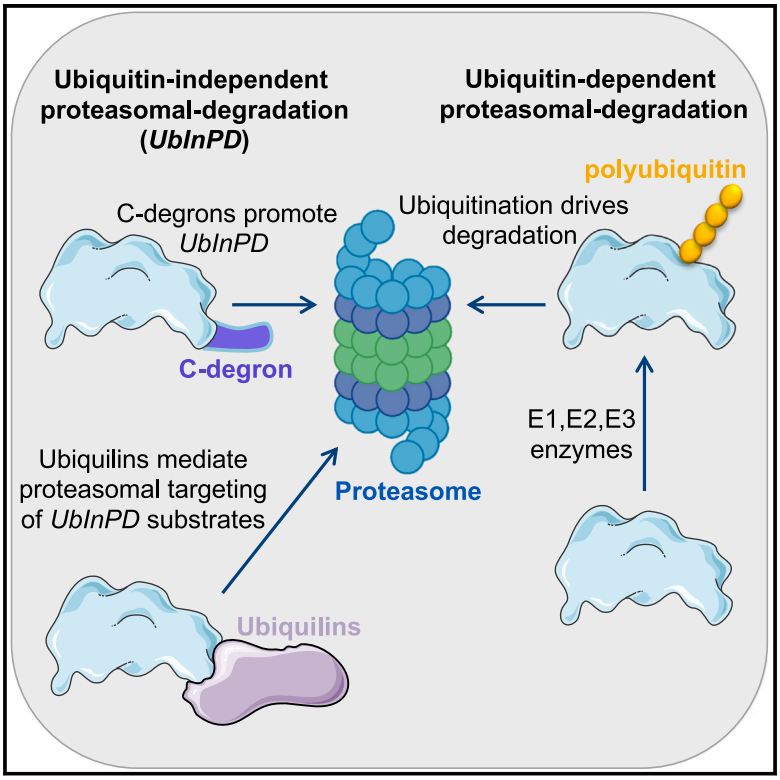

Highlights

- C-degrons can promote ubiquitin-independent proteasomal degradation (*UbInPD*)
- *UbInPD* is more prevalent than currently appreciated
- *UbInPD* performs both regulatory and protein quality control functions
- Ubiquilin family proteins are involved in the turnover of *UbInPD* substrates

Authors

Yaara Makaros, Anat Raiff, Richard T. Timms, ..., Michael H. Glickman, Stephen J. Elledge, Itay Koren

Correspondence

itay.koren@biu.ac.il

In brief

While the proteasomal degradation of most eukaryotic proteins is thought to be dependent on ubiquitin, Makaros et al. systematically investigated the requirements and mechanisms underlying protein degradation independent of ubiquitination. They found that C-terminal motifs and shuttling factors of the Ubiquilin family promote ubiquitin-independent proteasomal degradation (*UbInPD*).

Makaros et al., 2023, Molecular Cell *83*, 1921–1935
June 1, 2023
https://doi.org/10.1016/j.molcel.2023.04.023

CellPress

Molecular Cell

CellPress
OPEN ACCESS

Resource

Ubiquitin-independent proteasomal degradation driven by C-degron pathways

Yaara Makaros,[1] Anat Raiff,[1] Richard T. Timms,[2] Ajay R. Wagh,[3] Mor Israel Gueta,[1] Aizat Bekturova,[1] Julia Guez-Haddad,[1] Sagie Brodsky,[4] Yarden Opatowsky,[1] Michael H. Glickman,[3] Stephen J. Elledge,[5] and Itay Koren[1,6,*]

[1]The Mina and Everard Goodman Faculty of Life Sciences, Bar-Ilan University, Ramat-Gan 5290002, Israel
[2]Cambridge Institute of Therapeutic Immunology and Infectious Disease, Jeffrey Cheah Biomedical Centre, Cambridge Biomedical Campus, Cambridge, Cambridgeshire CB2 0AW, UK
[3]Faculty of Biology, Technion-Israel Institute of Technology, Haifa 3525433, Israel
[4]Department of Molecular Genetics, Weizmann Institute of Science, Rehovot 7610001, Israel
[5]Department of Genetics, Harvard Medical School, Division of Genetics, Brigham and Women's Hospital, Howard Hughes Medical Institute, Boston, MA 02115, USA
[6]Lead contact
*Correspondence: itay.koren@biu.ac.il
https://doi.org/10.1016/j.molcel.2023.04.023

SUMMARY

Although most eukaryotic proteins are targeted for proteasomal degradation by ubiquitination, a subset have been demonstrated to undergo ubiquitin-independent proteasomal degradation (*UbInPD*). However, little is known about the molecular mechanisms driving *UbInPD* and the degrons involved. Utilizing the GPS-peptidome approach, a systematic method for degron discovery, we found thousands of sequences that promote *UbInPD*; thus, *UbInPD* is more prevalent than currently appreciated. Furthermore, mutagenesis experiments revealed specific C-terminal degrons required for *UbInPD*. Stability profiling of a genome-wide collection of human open reading frames identified 69 full-length proteins subject to *UbInPD*. These included REC8 and CDCA4, proteins which control proliferation and survival, as well as mislocalized secretory proteins, suggesting that *UbInPD* performs both regulatory and protein quality control functions. In the context of full-length proteins, C termini also play a role in promoting *UbInPD*. Finally, we found that Ubiquilin family proteins mediate the proteasomal targeting of a subset of *UbInPD* substrates.

INTRODUCTION

The ubiquitin-proteasome system (UPS) represents the major route by which the cell degrades unwanted proteins.[1] In the canonical mode of protein degradation, the conjugation of ubiquitin to substrates serves as the signal for proteasomal targeting and subsequent degradation.[2,3] Ubiquitination occurs through a cascade of three enzymes, whereby ubiquitin activated by the E1 enzyme is transferred to an E2 ubiquitin-conjugating enzyme and then finally to the target substrate recruited by an E3 ligase.[4] E3 ligases play a crucial role in providing specificity[5] by interacting with their substrates through the direct recognition of short peptide motifs termed degrons. Degrons are defined as the minimal element that is sufficient for recognition and degradation by the proteolytic machineries, and an important property of degrons is that they are transferable.[6,7]

A small number of eukaryotic proteins have been demonstrated to undergo ubiquitin-independent proteasomal degradation (*UbInPD*). Best characterized is the enzyme ornithine decarboxylase (ODC).[8,9] ODC was long regarded as an unusual exception, but a handful of other cellular proteins, including p53, p21, Fos, and Rpn4[10–17] have since been proposed to undergo *UbInPD*, although in some cases this has been controversial.[18,19] For many of these proteins the evidence supporting ubiquitin-independent degradation was obtained *in vitro*, and hence, the biological relevance of this degradation remains unclear; indeed, the physiological degradation of some of these proteins strongly depends on ubiquitin. Moreover, there is increasing evidence that, within the same cell and under the same conditions, different pools of the same protein can be addressed to the proteasome via both ubiquitin-dependent and ubiquitin-independent mechanisms.[18,19]

Over the years efforts have been made to characterize the molecular mechanisms by which substrates undergoing *UbInPD* are targeted to the proteasome. However, given the relatively small number of substrates identified, conclusions have inevitably been drawn on a case-by-case basis. Intrinsically disordered regions[19] and defined sequence motifs,[9,15,20–22] including hydrophobic residues,[23,24] within substrates have been shown to promote proteasomal targeting. Furthermore, although the existence of the *UbInPD* has been appreciated for some time, it remains unclear whether the handful of known

UbInPD substrates are representative of all classes of substrates, or whether a wider range of additional substrates await discovery.

Here, we utilized global protein stability (GPS)-peptidome technology[25] to systematically identify human protein sequences that promote *UbInPD*. We find thousands of peptide substrates that undergo *UbInPD*, providing *in vivo* evidence that cells can target multiple substrates for proteasomal degradation in a manner independent of ubiquitin. Mutagenesis experiments on hundreds of peptides mapped consensus sequences underlying *UbInPD* and identified specific motifs located at the extreme C termini of proteins that mediate *UbInPD*. Moreover, a GPS-ORFeome screen with a large collection of human open reading frames (ORFs) identified novel full-length protein substrates that are subject to *UbInPD*, some of which required their C terminus and shuttling factors of the Ubiquilin family for *UbInPD*. Overall, our study represents a systematic approach to investigate substrate selection for *UbInPD*, which has implications for our understanding on the evolution of degradative mechanisms from prokaryotes to eukaryotes.

RESULTS

Identifying C-terminal motifs in the human proteome that promote *UbInPD*

To systematically investigate specificity of degradation in the UPS, we recently developed a high-throughput platform for degron identification named GPS-peptidome.[25,26] GPS-peptidome is a hybrid of the GPS technology, a method that systematically measures protein stability[27] combined with a synthetic representation of the human peptidome (Figure S1A). Exploiting a GPS-peptidome library that encoded the last 23 residues of all human proteins (hereafter "GPS-C23mer") allowed us to map a suite of degrons located at the C termini of human proteins ("C-degrons").[25]

While the majority of C-degrons that we identified were regulated by the Cullin-RING ligases (CRLs)[25] family, a handful of bona fide C-degrons, such as alanine at either the terminal position (A-1) or at the penultimate position (A-2), and valine at the penultimate position (V-2), were not.[25] To characterize the mode of degradation of substrates bearing these motifs, we studied three example substrates in which the C-terminal 23 residues (hereafter "C23mer") of CPS1 (A-1), SREBF2 (A-2), and OR4C13 (V-2) were fused to green fluorescent protein (GFP). To inhibit ubiquitination, we used the small-molecule MLN7243 that potently inhibits the mammalian E1 enzymes.[28] Treatment of human embryonic kidney (HEK)293T cells (1 μM for 6 h) efficiently blocked E1 activity and eliminated ubiquitin conjugation (Figure 1A). We then monitored the stability of the GFP-fusions of CPS1, SREBF2, and OR4C13 in cells treated with MLN7243 or the proteasome inhibitor bortezomib. In these assays, the C-terminal 37 residues of mouse ODC (mODC) or the C23mer from MAGEA6 fused to GFP served as positive controls representing ubiquitin-independent[21] or ubiquitin-dependent proteasomal substrates,[25,29] respectively. Intriguingly, similar to mODC, the stability of the GFP-fusions increased in response to bortezomib, but remained unchanged or even decreased following MLN7243 treatment (Figure 1B). In contrast, MAGEA6 was stabilized with both inhibitors (Figure 1B). Analysis of stability in cells simultaneously treated with MLN7243 and bortezomib revealed that no residual ubiquitination was detected even in cells treated with both drugs (Figure 1C) and that the turnover of the GFP-peptide substrates was still dependent on the proteasome in E1-inhibited cells (Figure 1D). Taken together with our previous findings, which showed that mutation of the terminal alanine or valine residues resulted in stabilization,[25] these data suggest that these C-terminal motifs can promote proteasomal degradation independently of ubiquitination.

To systematically search for additional C-degrons promoting *UbInPD*, we screened the GPS-C23mer library (Figure S1A) in cells treated with either bortezomib, MLN7243, or left untreated for 6 h. In the bortezomib-treated cells, we observed a dramatic global increase in the stability of the GFP-peptide fusions, as indicated by a large decrease in the percentage of cells in the lower stability bins (Figure S1B). Conversely, a far less pronounced effect was seen upon treatment with MLN7243 (Figure S1B), indicating that, for many of the unstable peptides, their proteasomal degradation was not dependent on ubiquitination. Following fluorescence-activated cell sorting (FACS) into 6 bins based on stability of GFP-fusions, the stability of each fusion was quantified by Illumina sequencing, with each peptide assigned a protein stability index (PSI) score according to the proportion of sequencing reads in each bin (Figure S1A; Table S1). Substrates were considered to undergo *UbInPD* if they exhibited significant stabilization with bortezomib treatment but showed no stability change in response to MLN7243; conversely, we considered substrates stabilized by both bortezomib and MLN7243 as ubiquitin-dependent (see STAR Methods).

Altogether, we identified 1,829 ubiquitin-independent and 2,121 ubiquitin-dependent proteasomal substrates (Table S1). GPS screen profiles for the *UbInPD* substrates CPS1, OR4C13, SREBF2, and ODC are presented in Figure S1C. The performance of CRL substrates[25] is shown in Figure S1D; these serve as control ubiquitin-dependent proteasomal substrates. Overall, the average PSI of the ubiquitin-independent substrates (2.78) was very similar to that of the ubiquitin-dependent substrates (2.72), suggesting that proteasomes control the turnover of peptide substrates equally well regardless of their ubiquitination state.

UbInPD driven by C-terminal peptides is transferable

We validated the screen results by examining the response of 13 individual *UbInPD* GFP-peptide substrates to the inhibitors. All peptides were stabilized in proteasome-inhibitor-treated cells but degraded even more efficiently in E1 inhibitor-treated cells (Figures 2A and S2A). These data suggest that there might be competition among substrates, such that, upon E1 inhibition, greatly decreased flux through the proteasome increases the capacity for the degradation of *UbInPD* substrates. Finally, to exclude cell-line-specific effects, we repeated the experiments in another human cell line, U2OS (Figure 2B), and in the mouse epithelial cell line, mouse Inner Medullary Collecting Duct-3 (mIMCD-3) (Figure 2C). These experiments showed that this mode of degradation is not specific to HEK293T cells.

To show that the degrons mediating *UbInPD* are transferrable, we fused example *UbInPD* peptide substrates to the bacterial

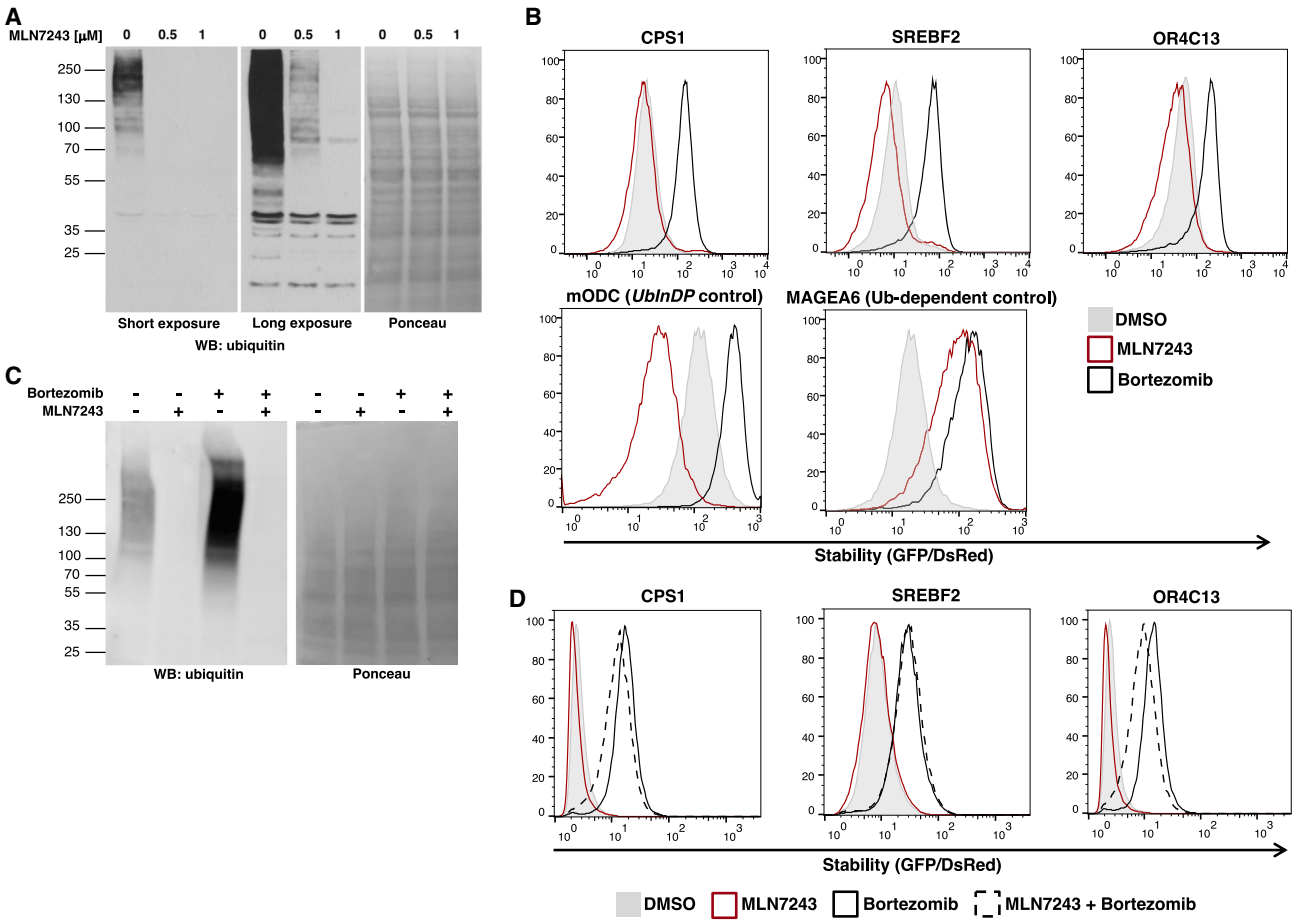

Figure 1. GFP-peptides are degraded by the proteasome independent of ubiquitination

(A) Ubiquitination is attenuated in E1-inhibited cells. HEK293T cells were treated with 0.5 or 1 μM MLN7243 for 7 h, and the abundance of ubiquitin conjugates assessed by western blot (WB) using the FK2 anti-ubiquitin antibody. Ponceau staining served as a loading control.

(B) Cells expressing GPS constructs in which GFP was fused to the last 23 residues of CPS1, SREBF2, OR4C13, or MAGEA6, or last 37 residues of mouse ODC (mODC), were treated with vehicle control (DMSO), 1 μM MLN7243 or bortezomib for 7 h and analyzed by flow cytometry. The GFP/dsRed ratio represents the stability of the indicated GFP-fusion proteins. Stabilization of the target protein by the indicated inhibitors is indicated by a sharp peak to the right side of each panel.

(C and D) HEK293T cells were treated with 1 μM MLN7243, 10 μM bortezomib, or 1 μM MLN7243 plus 10 μM bortezomib for 6 h. Ubiquitin-conjugated substrates abundance was assessed by WB using the VU-0101 anti-ubiquitin antibody (C), and the stability of the GFP-fusion proteins was assessed by flow cytometry (D).

protein BirA[30] and monitored protein levels by western blot: all of the peptides conferred instability (Figure S2B). As with the equivalent GFP-fusions, MLN7243 treatment resulted in reduced protein levels, while bortezomib treatment increased the protein levels; TSPYL1, an endogenous ubiquitin-dependent CRL substrate[25] was stabilized with both inhibitors (Figure S2B). Thus, these peptides function autonomously: transplantation was sufficient to convert a stable protein into a *UbInPD* substrate.

Ubiquitin conjugation in mammals is initiated by UBA1 and UBA6, with UBA1 responsible for charging >99% of cellular ubiquitin.[31] At 1 μM, MLN7243 inhibits UBA1 and UBA6 with equal potency in cells.[28] However, to exclude the possibility that proteasomal degradation was mediated by residual ubiquitination via UBA6, we generated UBA6 knockout (KO) cells by CRISPR-Cas9 (Figure S2C) and monitored the stability of representative substrates. UBA6 ablation did not have any effect on the stability of the *UbInPD* substrates (Figure S2D), suggesting that the turnover of *UbInPD* substrates is not regulated by UBA6.

C-terminal motifs define the minimal elements driving *UbInPD*

Notably, sequence analysis of the C termini of ubiquitin-independent versus ubiquitin-dependent substrates revealed enrichment of Ala-end (A-1, A-2, and A-3), Cys-end (C-1, C-2, and C-3), and Val-end (V-1, V-2, V-3, and V-4) motifs (Figure 3A). The median stability of C23mer peptides containing these motifs was significantly increased in bortezomib-treated cells ($p < 1e^{-68}$) and decreased in response to MLN7243 treatment ($p < 1e^{-8}$) (Figure 3B), indicating of the involvement of these C-terminal motifs in directing *UbInPD*. Overall, the median stability score of all peptides in the C23mer library harboring these motifs at their specific C-terminal location was lower compared

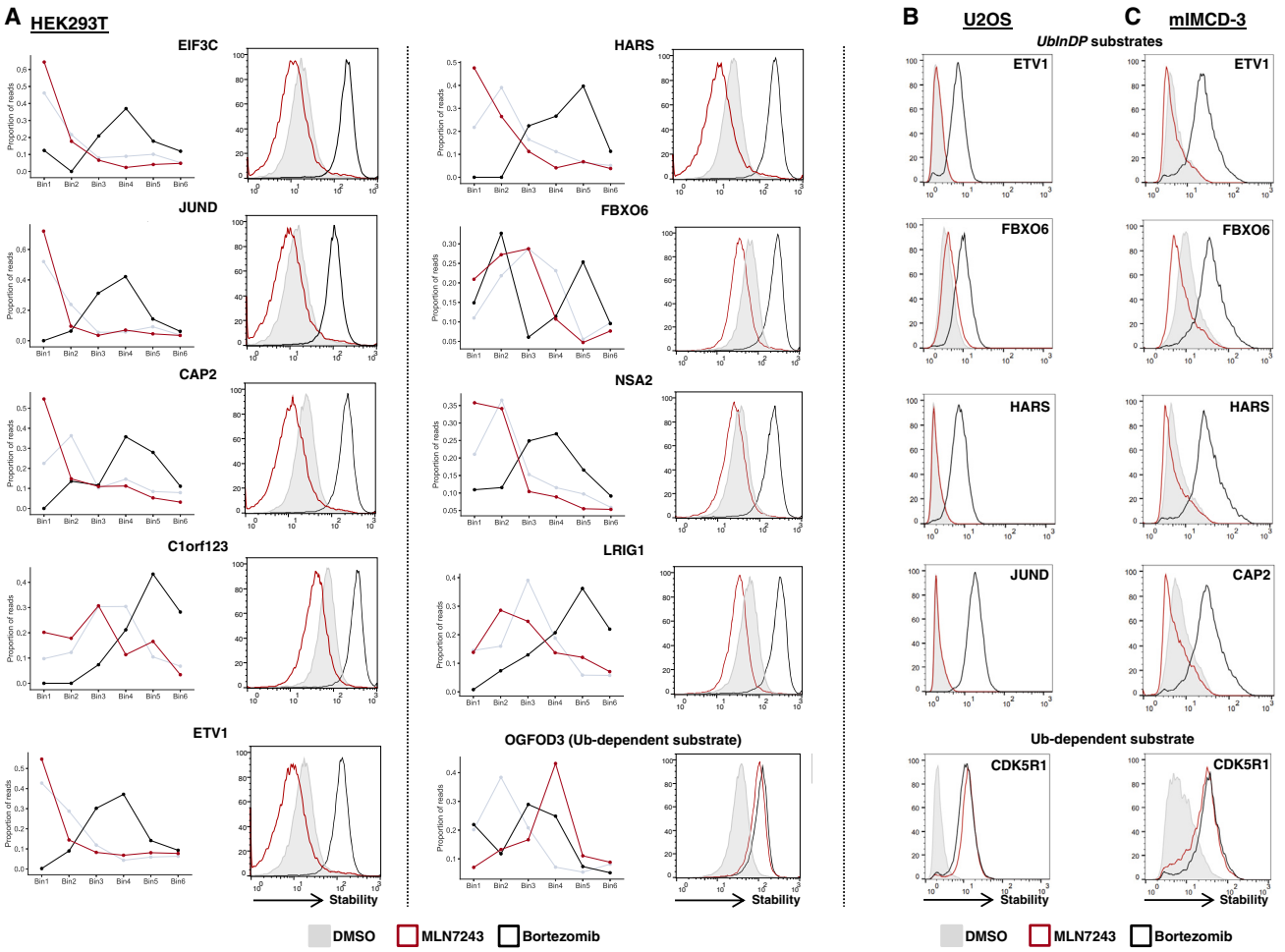

Figure 2. GPS-peptidome screen identifies *UbInPD* substrates

(A) For each of the indicated GFP-C23mers, the GPS screen profiles (representing the distribution of sequencing reads across the bins in control treated cells (DMSO) versus MLN7243 or bortezomib treatments) are shown on the left, and individual validations as analyzed by flow cytometry following treatment with the indicated inhibitors for 7 h are shown on the right.

(B and C) U2OS cells (B) or mIMCD-3 cells (C) expressing GPS-C23mers of the indicated *UbInPD* substrates were treated with 1 μM MLN7243 or bortezomib for 7 h and analyzed by flow cytometry.

with peptides in which the motif was placed at any other location across the peptide (Figure 3C). Moreover, many of these motifs were computationally predicted to serve as destabilizing elements specifically when placed at the extreme terminus.[25] Altogether, these findings underscore that these C-end motifs promote instability specifically when placed at the extreme C terminus.

To experimentally map consensus motifs mediating *UbInPD*, we performed mutagenesis experiments on ~100 *UbInPD* peptide substrates. In this set of experiments, we generated mutant peptide libraries in which single amino acids scanning across all positions within the 23mer were substituted to a distinct amino acid. As in some cases single amino acid substitutions may not be sufficient to disrupt degron activity, we also generated triple substitution mutants (in which three successive amino acids were mutated) and triple deletion mutants (in which three successive amino acids were deleted). The three mutagenesis libraries were screened in the context of the GPS system, as described above (Figure S1A). The mutagenesis revealed that indeed Ala-end, Cys-end, and Val-end are involved in peptide degradation: mutation or deletions of these residues promoted increased stability of the substrates (Figure 3D; Table S2). In addition to these motifs, C-terminal motifs composed of short stretches of hydrophobic residues were also revealed (Figure 3D, see SHROOM1, OAT and FBXO6). In ~90% of cases, the identified motifs were located at the extreme C terminus of the 23mer (Figure 3D; Table S2); in rare cases, however, the motif was located in the middle or beginning of the 23mer (Figure S3A). Furthermore, for two example Ala-end peptides, we defined the *UbInPD* degron in detail by performing saturation mutagenesis experiments. We created a library in which each of the residues across the 23-amino-acid peptide were mutated to all other possible amino acids and performed the GPS screens as detailed above

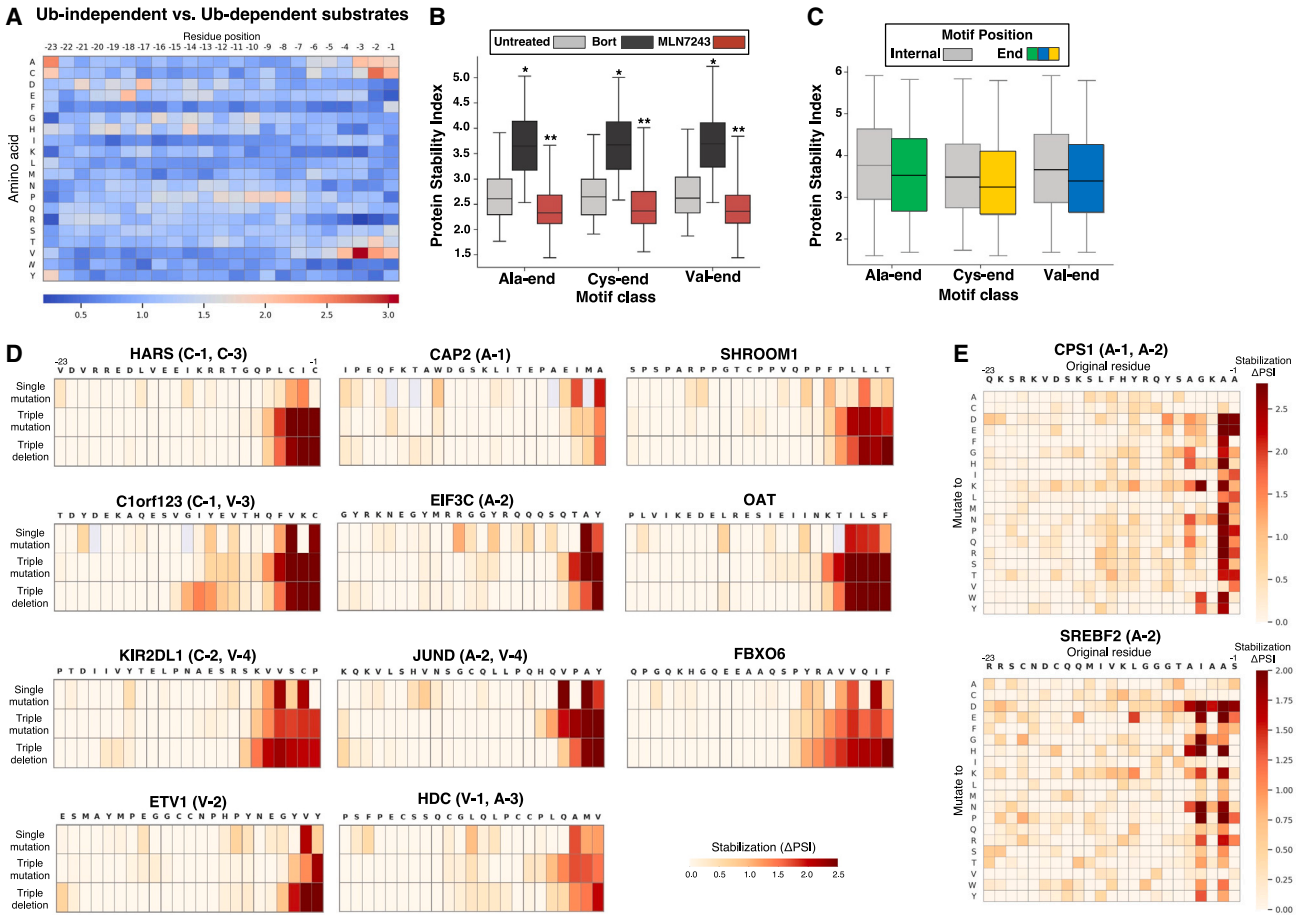

Figure 3. Specific C-terminal motifs are enriched among *UbInPD* substrates

(A) Heatmaps showing the relative depletion (blue) or enrichment (red) of each amino acid across all positions of the 23mer peptide, comparing ubiquitin-independent substrates with ubiquitin-dependent substrates.

(B) Boxplots showing the distribution of PSI scores for all *UbInPD* peptides harboring the indicated C-terminal motifs in untreated, bortezomib (Bort) or MLN7243 treated cells. Motifs were grouped as follows: Ala-end (A-1, A-2, and A-3), Cys-end (C-1, C-2, and C-3), and Val-end (V-1, V-2, V-3, and V-4). *$p < 1e^{-68}$ and **$p < 1e^{-8}$ denote statistical significance comparing untreated with bortezomib or MLN7243, respectively (*t* test, see STAR Methods).

(C) Boxplots showing the distribution of PSI scores for all peptides harboring the indicated classes of motif internally within the 23mer peptide (gray boxes) or specifically at the C terminus (colored boxes).

(D) Scanning mutagenesis of *UbInPD* substrates. For each of the indicated genes, three independent mutagenesis experiments were performed: mutagenesis of single residues (top), mutagenesis of three consecutive residues (middle), and deletion of three consecutive residues (bottom). In each case, darker colors represent a greater degree of stabilization conferred by the mutation/deletion. Name of the gene is indicated, and the critical C-terminal residues regulating stability are shown in brackets. A universal scale of stabilization is shown at the bottom.

(E) Saturation mutagenesis was performed for two *UbInPD* substrates. Each residue across the 23mer peptide was mutated to all other possible amino acids, and the stability of the resulting GFP-peptide fusions was measured by means of FACS and Illumina sequencing. In each case, the darker the color, the greater the degree of stabilization as compared with that of the wild-type sequences.

(Figure S1A). These experiments confirmed the critical importance of the Ala residues encoded at the terminal positions but also demonstrated that certain mutations at the -4 or -5 position could prevent degradation (Figure 3E; Table S2). Interestingly, the only residues other than Ala in the terminal positions that still supported degradation were Cys and Val, the two other residues found to be enriched in C termini of *UbInPD* substrates (Figures 3A–3C). Repositioning of the terminal motif by adding additional amino acids at the C terminus ("+tail") lead to marked stabilization of all peptides tested (Figure S3B), indicating the importance of the motif being exposed at the C terminus to promote *UbInPD*. Thus, it is not only the sequence composition that is important to drive *UbInPD* but also the position of the degron motif at the extreme C terminus. Altogether, these data suggested that *UbInPD* is primarily (but not exclusively) mediated through C-degrons.

Ubiquitination is not required for proteasomal degradation of *UbInPD* substrates bearing C-degrons

To confirm that the candidate *UbInPD* substrates were not ubiquitinated in cells, we monitored the ubiquitination levels of representative substrates fused to GFP. In this set of experiments an

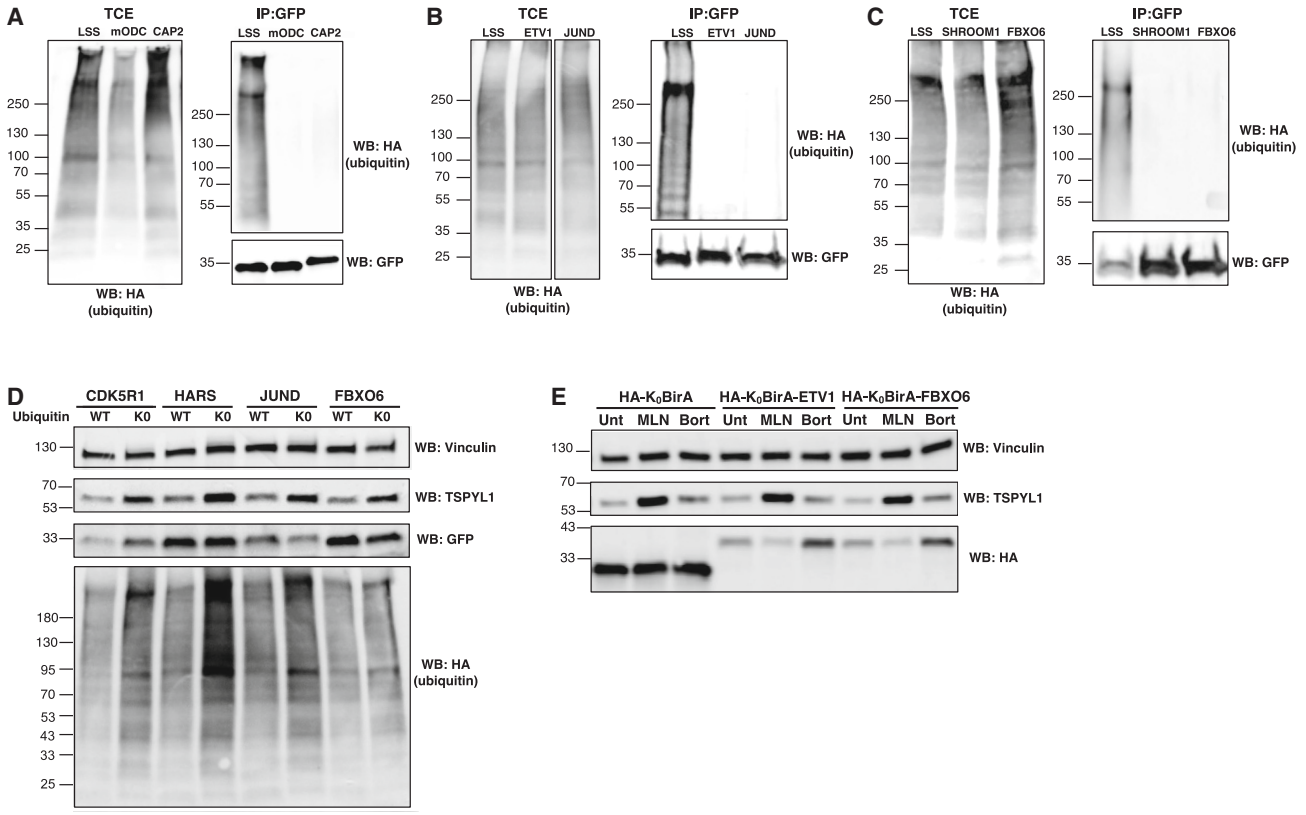

Figure 4. *UbInPD* substrate turnover is ubiquitination-independent

(A–C) Ubiquitin conjugates are not detected on *UbInPD* substrates immunoprecipitated from cells using anti-GFP beads. The ubiquitination status of GFP-fused mODC and the C23mer from CAP2 are shown in (A), C23mers from ETV1 and JUND in (B), and C23mers from SHROOM and FBXO6 in (C). LSS represents a ubiquitin-dependent substrate that is heavily ubiquitinated when purified from cells. Immunoblot analysis was performed on both total cell extracts (TCEs) and immunoprecipitated (IP) GFP using anti-HA antibody to detect HA-ubiquitin conjugates. Anti-GFP antibody was used to show equal GFP pull downs across samples.

(D) HEK293T cells expressing GFP-C23mers of *UbInPD* substrates HARS, JUND, FBXO6, and the ubiquitin-dependent substrate CDK5R1 were transfected for 24 h with HA-tagged wild-type (WT) or lysine-less ubiquitin (K0). Cell extracts analyzed using antibodies against GFP, HA, and TSPYL1. Vinculin served as a loading control.

(E) HEK293T cells were transduced with HA-tagged lysine-less BirA alone (K_0BirA) or fused to the C23mer *UbInPD* substrates FBXO6 or ETV1. Following 6 h treatment with MLN7243 (MLN) or bortezomib (Bort) cells were harvested for western blot. HA-K_0BirA abundance was assessed by immunoblot with HA antibody while vinculin antibody was used as a loading control. The protein levels of TSPYL1, a ubiquitin-dependent substrate were monitored with endogenous TSPYL1 antibody. FBXO6 and ETV1 C23mers do not encode lysine.

artificial GFP-fused C-terminal hydrophobic degron,[32] hereafter named "LSS," served as ubiquitin-dependent proteasome-dependent control peptide substrate (Figure S4A). Indeed, LSS purified from cells was heavily ubiquitinated, while mODC and all of the *UbInPD* peptide substrates examined were not (Figures 4A–4C).

Another measure for asserting that prior ubiquitination is not required for proteasomal degradation is the absence of stabilization upon overexpression of a lysine-less (K0) non-polymerizable ubiquitin variant. Transient overexpression of lysine-less ubiquitin resulted in the stabilization of well-established ubiquitin-dependent substrates,[25] including endogenous proteins (Figure S4B) as well as the GFP-fused C23mer from CDK5R1 (Figure 4D). Conversely, none of the *UbInPD* C23mers substrates were stabilized under these conditions, and again if anything were further destabilized (Figure 4D), similar to the destabilization observed in MLN7243-treated cells (Figures 1B and 2A). Furthermore, *UbInPD* peptides were still degraded by the proteasome when fused to a BirA model substrate in which ubiquitin acceptor sites were eliminated by mutating internal lysines to arginine and N-terminal ubiquitination was prevented by an HA peptide tag (referred to as K_0BirA). Similar to wild-type (WT) BirA fused to example *UbInPD* C23mers (Figure S2B), K_0BirA fusions promoted instability and were degraded (even more efficiently) by the proteasome in E1-inhibited cells (Figure 4E).

Altogether, the absence of *in vivo* ubiquitination, the lack of stabilization observed upon inhibition of E1 enzymes, and the lack of effect upon expression of lysine-less ubiquitin variants or after eliminating substrate ubiquitin acceptor sites suggests that ubiquitination is not required for the proteasomal degradation of these GFP-fusion peptide substrates.

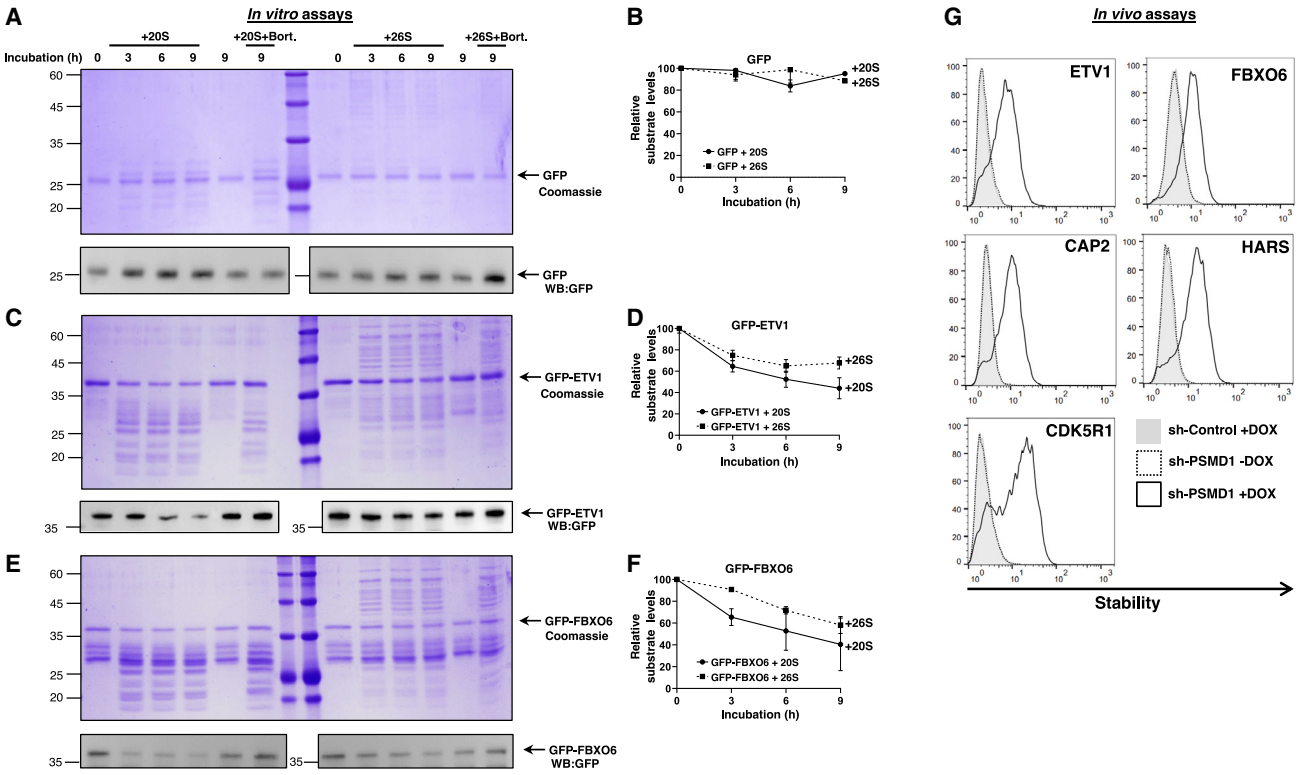

Figure 5. *UbInPD* substrates are proteolyzed by both 20S and 26S proteasomes *in vitro* but are mostly degraded by 26S proteasomes *in vivo*

(A–F) *UbInPD* substrates are degraded by purified proteasomes *in vitro*. Recombinant GFP (A and B), GFP-ETV1 (C and D), or GFP-FBXO6 (E and F) were incubated with purified 20S or 26S proteasomes for 3–9 h followed by analysis using Coomassie stain and western blot with anti-GFP antibody. Bortezomib (+Bort) was added to show that degradation is dependent on the catalytic activity of the proteasomes. Quantification of the degradation (based on three independent experiments) is presented in (B), (D), and (F).

(G) *UbInPD* substrates are degraded by 26S proteasomes *in vivo*. Cells expressing inducible shRNAs against either luciferase (sh-control) or PSMD1 (sh-PSMD1) were transduced with the indicated GPS-C23mers, and their stability was analyzed by flow cytometry following 3 days of doxycycline (+DOX) treatment.

20S and 26S proteasomes are able to proteolyze *UbInPD* substrates *in vitro*

In vitro, both 20S, and 26S proteasomes have been shown to mediate selective degradation of *UbInPD* substrates.[18,19] To examine the requirements for the degradation of GFP-fusion *UbInPD* peptide substrates, we performed *in vitro* degradation assays with purified 20S or 26S proteasomes. As expected, two model 20S and 26S substrates, the N terminus of cyclin B1 (CyB1-NT) fused to GST[33] and β-casein,[34] respectively, were efficiently proteolyzed by purified proteasomes *in vitro* (Figures S4C–S4F), while GFP alone was not (Figures 5A and 5B). Two example GFP-C23mers subject to *UbInPD*, derived from ETV1 and FBXO6, were proteolyzed by both purified 20S and 26S proteasomes, with faster kinetics observed with 20S (Figures 5C–5F). Thus, peptides fused to GFP can serve as both the targeting signal and the initiation site to mediate proteasomal degradation.

To distinguish between degradation by 20S versus 26S proteasomes in cell-based assays, we analyzed the stability of the GFP-fused peptide substrates in cells expressing an inducible small hairpin RNA (shRNA) targeting Proteasome 26S subunit, non-ATPases 1 (PSMD1). PSMD1 is required for degradation by the 26S proteasome, but not the 20S proteasome, and hence upon doxycycline treatment, PSMD1 depletion results in the attenuation of degradation by the 26S proteasome.[35] All peptides tested were significantly stabilized in PSMD1-depleted cells, indicating that *in vivo* degradation of these *UbInPD* substrates depends on 26S and not 20S proteasomes (Figure 5G).

Finally, to assess the involvement of 20S versus 26S proteasomes in the degradation of *UbInPD* substrates globally, we analyzed the stability of the entire C-terminome library upon silencing of PSMD1 (Figure S4G). PSMD1 depletion resulted in significant stabilization of *UbInPD* GFP-peptide fusions, suggesting that most, if not all, *UbInPD* substrates recovered from our screen are 26S proteasome substrates *in vivo*.

Identification of full-length proteins subject to *UbInPD*

To elucidate the biological significance and molecular mechanism of *UbInPD*, we were interested in identifying full-length protein substrates. To this end, we used a barcoded library of ~15,000 ORF constructs encoding full-length human proteins cloned into the GPS vector[25] (Figure S5A) and performed a GPS experiment in library expressing cells sorted into four bins following MLN7243 or bortezomib treatment (Figure S5B; Table S3). This approach identified 69 full-length ORFs as

candidate *UbInPD* substrates (Table S3). Representative histograms of ubiquitin-independent and ubiquitin-dependent candidates are presented in Figure S5C and Figure S5D, respectively. These included established *UbInPD* substrates such as Fos[15,36] and the ubiquitin-like (UBL) and ubiquitin-associated (UBA) domain-containing protein, Ubiquilin Like (UBQLNL).[37] The relatively small number of substrates compared with the peptidome screen suggests that, in the context of full-length proteins, only a specific subset of proteins are degraded in a ubiquitin-independent manner.

Interestingly, ~60% of the *UbInPD* candidate substrates are membrane or secreted proteins (Table S3), representing a significantly enrichment ($p < 0.001$, chi-squared test) compared with the 37% of these proteins present in our GPS-ORFeome collection. Indeed, database for annotation, visualization, and integrated discovery (DAVID) functional annotation analysis[38,39] revealed a significant 1.6-fold enrichment ($p < 0.05$) of "transmembrane helix" annotation among *UbInPD* substrates (Table S4). Among the candidate substrates of the secretory pathway, 43% contain an N-terminal signal peptide (Table S3). Since in the context of the GPS construct GFP is fused at the N terminus of the ORF, thus masking any signal peptide, secretory proteins will not be able to translocate across membranes and thus are presumably mislocalized to the cytosol. Three additional proteins are mitochondria proteins (Table S3) for which GFP-fusion might interfere with transit peptide localization into mitochondria. Thus, *UbInPD* might serve as a protein quality control (PQC) mechanism to eliminate mislocalized proteins. Disorder tendency does not seem to play a role in the selection of full-length substrates, as we found no significant difference between the median disorder score calculated by IUPred[40] of *UbInPD* substrates compared with the library ($p = 0.68$, *t* test) (Figure S5E; Table S5).

To validate full-length candidates, we chose nine ORFs and cloned them individually into the GPS vector. These candidates all scored as *UbInPD* substrates in the GPS-ORF screen (Table S3) and exhibited high concordance between individually barcoded replicates (Figure S5C). In addition, they represent proteins located in either the cytoplasm (UBQLNL and Neuronatin [NNAT]), the nucleus (REC8 and Cell Division Cycle Associated 4 [CDCA4]), or both (BTG2). We also selected several membrane proteins that are mislocalized to the cytosol when expressed as C-terminal fusions to GFP in the context of the GPS system (Figure S5F): LRRN4 C-Terminal Like (LRRN4CL) and Glutamate Receptor Ionotropic Delta-1 (GRID1) contain N-terminal signal peptide, naked cuticle homolog 2 (NKD2) is N-terminally myristoylated,[41] and ATP Binding Cassette Subfamily C Member 5 (ABCC5) (isoform II) harbors a truncated transmembrane domain. All ORFs were stabilized in bortezomib-treated cells, but their stability either did not change (ABCC5, NKD2, BTG2, CDCA4, REC8, and LRRN4CL) or was only modestly enhanced (UBQLNL, GRID1, and NNAT) upon treatment with MLN7243 (Figure 6A). These results were not cell line dependent, as they were recapitulated in U2OS cells (Figure S6A). As with the peptide substrates, proteasomal degradation was independent of UBA6 (Figure S6B), was not impaired upon expression of lysine-less ubiquitin (Figure 6B), and, in E1-inhibited cells, degradation was dependent on the proteasome (Figure S6C).

Next, we validated the full-length substrates independently of GFP-fusions using an orthogonal approach. As effective commercial antibodies were not available, we generated expression constructs with N-terminal HA epitope tag fusions in a lentiviral backbone. HEK293T cells containing single copy integrants were monitored by western blot to measure the levels of the proteins in lysates made from cells treated with MLN7243 or bortezomib. As expected, RBM38, a known ubiquitin-dependent substrate,[25] was stabilized with bortezomib and MLN7243 to the same degree. For all of the candidate *UbInPD* ORFs, their protein abundance was increased in bortezomib-treated cells compared with controls, indicating that their turnover depends on the proteasome (Figure 6C). In response to MLN7243, however, REC8 and CDCA4 showed no increased protein levels and NKD2 showed reduced protein levels (Figure 6C). Thus, NKD2, CDCA4, and REC8 represent *UbInPD* substrates. BTG2 and ABCC5 exhibited some stabilization in response to MLN7243, suggesting that they may be partially targeted for degradation in a ubiquitin-independent manner (Figure 6C).

C-degrons play a role in *UbInPD* of full-length proteins

The C-terminal peptides derived from approximately 30% of the full-length candidates scored as *UbInPD* substrates in the C23mer screen (Table S1), which is significantly more than expected by chance ($p < 1e^{-5}$, hypergeometric test). The stability profiles of example C23mer peptides (Figure S6D) strongly resemble the corresponding ORFs (Figure S6E), suggesting that stability regulation may be conferred by the C termini.

To examine whether the C terminus does play a role in *UbInPD* of full-length substrates, we either deleted (Figure S6F) or added extra residues (+tail) (Figure S6G) to their C terminus and assayed the impact on their stability. Interestingly the C-terminally mutated proteins exhibited stabilization upon treatment with both MLN7243 and bortezomib (Figures S6F and S6G), suggesting that those substrates were converted to ubiquitin-dependent proteasomal substrates upon C-terminal deletion or blockage. These findings raise the possibility that full-length proteins subject to *UbInPD* can be degraded in both a ubiquitin-independent and ubiquitin-dependent manner, and, hence, when one mode of degradation is attenuated, these substrates can be degraded in the other pathway.

Ubiquilins are involved in targeting of *UbInPD* substrates to the proteasome

Finally, we considered the mechanism by which *UbInPD* substrates may be directed to the proteasome. UBL-containing shuttling factors were demonstrated to bridge substrates to the proteasome by associating with the proteasomal ubiquitin receptors. In most cases, UBL-proteins also contain UBA domain to mediate targeting of ubiquitinated substrates to the proteasome.[42,43] In plants, however, it was shown that RAD23 family members and the extra-proteasome ubiquitin receptor, Rpn10, are able to mediate proteasomal destruction of specific substrates independent of ubiquitination.[44,45] We thus hypothesized that UBL domain-containing proteins might be involved in targeting of *UbInPD* substrates. To this end, we measured stability of various full-length ORFs in cells disrupted for RAD23A, RAD23B, and the Ubiquilin family members,

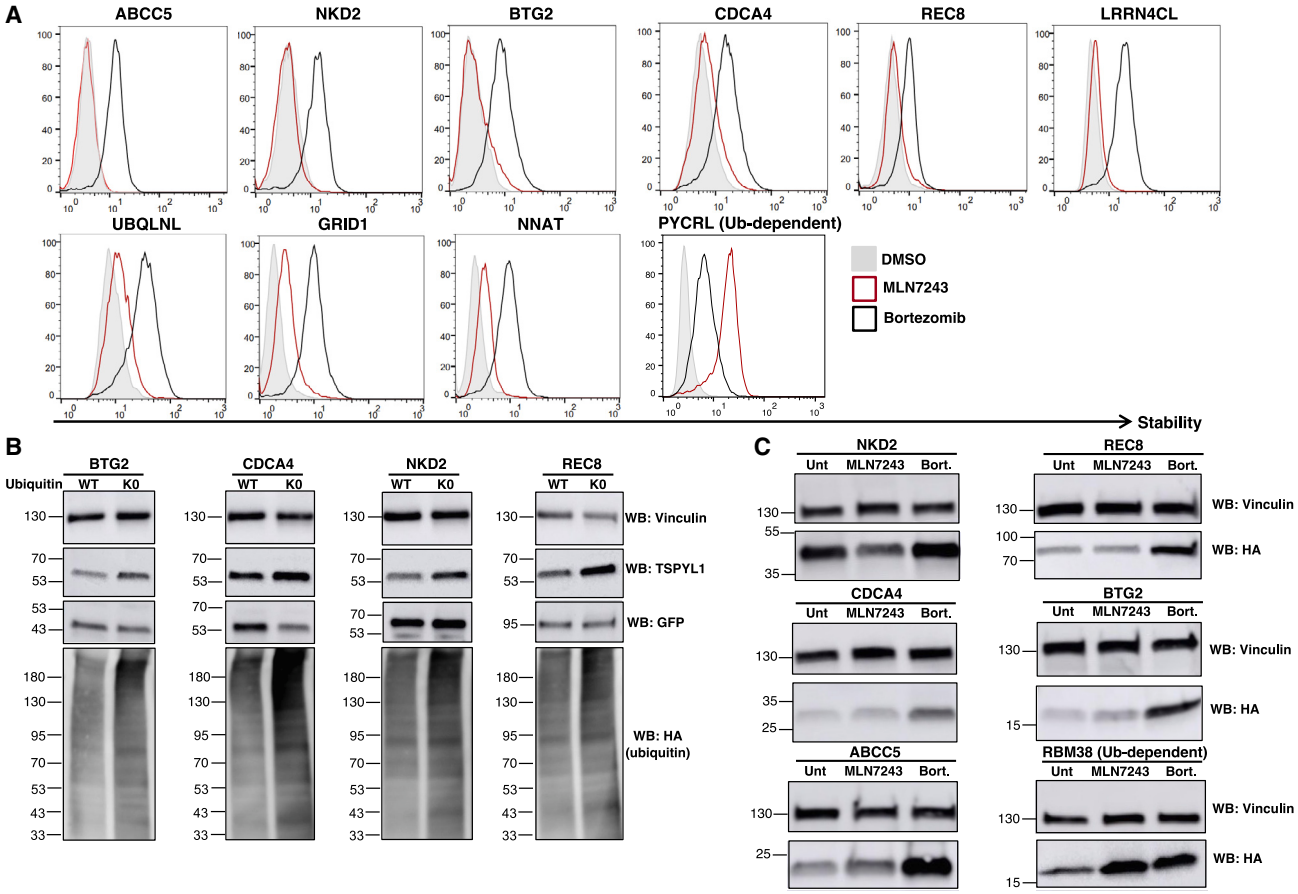

Figure 6. GPS-ORFeome screen identifies full-length *UbInPD* substrates

(A) The nine indicated *UbInPD* candidate full-length proteins were expressed as GFP-fusions in HEK293T cells and their stability was analyzed by flow cytometry following 7 h treatment with 1 μM MLN7243 or bortezomib.

(B) HEK293T cells expressing the indicated *UbInPD* substrates were transfected with HA-tagged wild-type (WT) or lysine-less ubiquitin (K0). 24 h post-transfection cells were harvested, and cell extracts analyzed by immunoblot.

(C) Five candidate *UbInPD* substrates were expressed as N-terminal HA epitope tag in HEK293T cells, and protein abundance assessed by immunoblot using anti-HA antibody following 6 h treatment with 1 μM MLN7243 or bortezomib (Bort).

UBQLN1, UBQLN2, and UBQLN4 (Figure S7A). Intriguingly, 3 out of 6 ORFs tested were substantial stabilized in these penta KO cells treated with MLN7243 (Figure 7A). This suggests that upon E1 inhibition, substrate degradation is dependent on the shuttling factors. None of the three substrates responded to RAD23A/B ablation (Figure 7B), but all were stabilized in Ubiquilins triple KO cells treated with MLN7243 (Figures 7C, S7B, and S7C). Therefore, Ubiquilin family members, but not RAD23 family members, play a role in the *UbInPD* of these substrates. Single ablation of each Ubiquilin member (Figure S7D) did not recapitulate the stabilization effect seen in the Ubiquilins triple KO cells, and only UBQLN1 disruption resulted in some degree of substrate stabilization (Figure S7E). Thus, although UBQLN1 might be the dominant member among the Ubiquilin family, it is likely that substantial redundancy exists between the family members in mediating destruction of *UbInPD* ORF substrates. Notably, under the same cellular settings, none of the tested GFP-fused peptides responded to ablation of the shuttling factors (Figure S7F).

To define the protein domain of Ubiquilins that promote *UbInPD*, we engineered UBQLN1 constructs lacking individual domains and performed genetic complementation experiments. Beside the UBL domain at the N terminus and the UBA domain at the C terminus, UBQLN1 also contains stress-induced protein-like (STI) motifs,[43] which confer chaperone-like functions.[46,47] The STI domains have been demonstrated to interact with hydrophobic regions of substrate proteins.[48,49] The rescue experiments showed that the UBA domain and STI-3/4 of UBQLN1 are not required for the *UbInPD* of the ORF substrates (Figure 7D); in contrast, however, the UBL or STI-1/2 deletion mutants could not rescue substrate stabilization (Figure 7D). The expression levels of various expressed UBQLN1 proteins were comparable judged by the western blot analysis (Figure 7E). Finally, we demonstrated a physical interaction between UBQLN1 and the *UbInPD* ORFs through co-immunoprecipitation experiments from cells (Figure 7F). Overall, this experiment suggests that, unlike the canonical function of Ubiquilin family members serving as

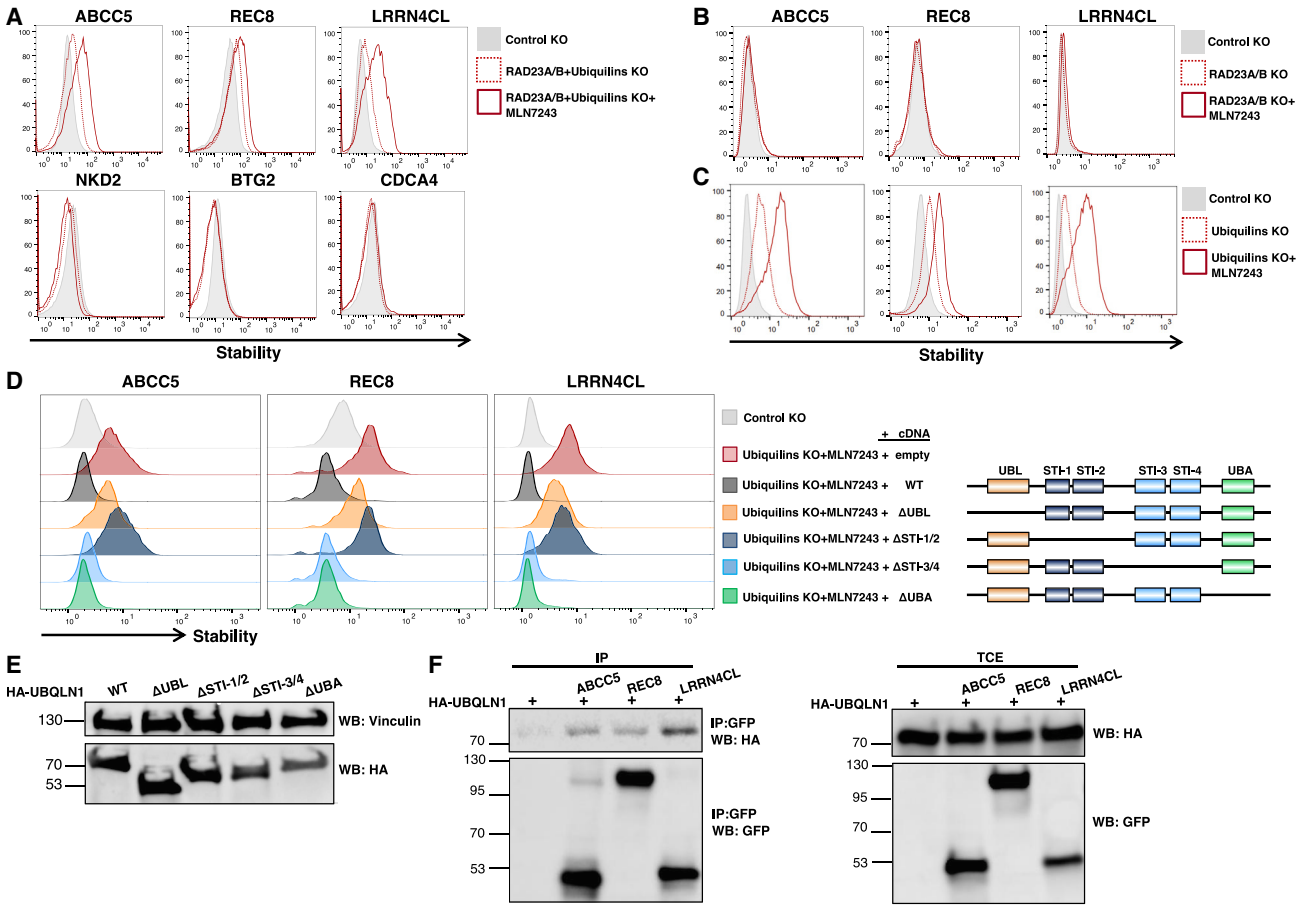

Figure 7. Stability of full-length *UbInPD* substrates is regulated by Ubiquilins

(A) Stability of the indicated *UbInPD* full-length ORFs as analyzed by flow cytometry in control KO (cells transduced with AAVSI-targeting single guide RNA [sgRNA]) or penta KO cells lacking RAD23A, RAD23B, and Ubiquilin 1, 2, and 4 in the presence or absence of 1 μM MLN7243.

(B and C) Stability analysis of the indicated GPS-ORFs in control KO cells or double KO cells lacking RAD23A and RAD23B (B), or triple KO cells lacking Ubiquilin 1, 2, and 4 (C) in the presence or absence of 1 μM MLN7243.

(D and E) The indicated GPS-ORFs were expressed in control KO or Ubiquilins triple KO cells that were transduced with either wild-type (WT) UBQLN1, or the indicated deletion mutants. 48 h post-transduction, stability analysis was performed by flow cytometry (D). Protein abundance of the transduced complementary DNAs (cDNAs) was assessed by immunoblot using HA antibody (E).

(F) HA-tagged UBQLN1 interacts with *UbInPD* GPS-ORFs *in vivo*. HEK293T cells stably expressing HA-tagged UBQLN1 with or without the indicated *UbInPD* GPS-ORFs substrates were generated. The GFP-fusions were immunoprecipitated from cells treated with 1 μM MLN7243 + 1 μM bortezomib followed by western blot analysis. GFP and HA antibodies are used to detect by immunoblot the GFP-fusions, and HA-tagged UBQLN1, respectively, in immunoprecipitation (IP) (left) and total cell extract (TCE) (right).

shuttling factor for ubiquitinated proteins via their UBA domain, Ubiquilins can also promote *UbInPD* of substrates through their chaperone-like STI domains.

DISCUSSION

It is currently thought that *UbInPD* is restricted to a handful of unusual proteins, and the mechanisms governing substrate recognition and proteasomal targeting remain largely unknown. However, *in vitro* degradation assays estimate that 20% of cellular proteins can be degraded independently of ubiquitination to some degree.[50] Here, we utilized the powerful GPS-peptidome approach to systematically search for *UbInPD* substrates and delineate C-terminal motifs promoting ubiquitination-independent proteasomal degradation. A high proportion of the ORF substrates also scored as *UbInPD* C-terminal peptides, suggesting the involvement of C-degrons in the context of the *UbInPD* of full-length proteins. We speculate that N-terminal sequences—or even exposed disordered internal regions—could in some circumstances function as degrons driving *UbInPD*.

UbInPD as a protein quality control mechanism

Our GPS-peptidome screens identified thousands of *UbInPD* substrates (~8% of the library) indicating that this mode of degradation is not limited to rare exceptions but rather can potentially promote the degradation of substantial fraction of the proteome. However, the fact that an ORFeome-wide screen identified only ~70 full-length substrates suggests that *UbInPD*

pathways may only normally handle a small fraction of the proteome, but under conditions of cellular stress, such as oxidative stress or heat shock, might be important to cope with increasing numbers of aberrant proteins. The artificial nature of the peptides in the context of the GPS-peptidome screen might thus mimic aberrant proteins exposing residues that can serve as *UbInPD* degrons.

Mislocalized membrane proteins represent another class of aberrant proteins that need to be handled by cellular PQC mechanisms. It has been shown that even under optimal conditions, a substantial fraction of secretory proteins fail to localize properly due to limited capacity of the targeting machinery. Moreover, mislocalization is often increased under conditions of stress, such as ER and mitochondrial stress.[51] The retention of secretory proteins in the cytoplasm leads to the exposure of hydrophobic residues of the transmembrane domains and signal sequences, resulting in aggregation that can lead to reduced cell viability. To this end, PQC pathways have evolved to deal with such aberrant proteins. Here, we found an enrichment of secretory proteins among *UbInPD* full-length substrates, suggesting that *UbInPD* might function as part of PQC mechanisms, either redundantly or in parallel to canonical ubiquitin-dependent pathways such as those operated by Bag6 and Ubiquilins.[48,52–54]

Molecular mechanisms of ubiquitin-independent substrate targeting to the proteasome

Interestingly, we found that degradation of example full-length *UbInPD* substrates was dependent on Ubiquilins. Although UBL-UBA proteins mostly interact with ubiquitinated proteins,[42,43] they might use other protein-protein interaction domains to interact with non-ubiquitinated substrates and promote their proteasomal degradation. For example, the methionine-rich domain of Ubiquilins, containing the STI regions, is able to interact directly with hydrophobic degrons to mediate substrate degradation.[48] Indeed, we found that the degradation of some full-length substrates subject to *UbInPD* was dependent on the Ubiquilins' STI-1/2 region and not on their UBA domain. However, the stability of three out of six *UbInPD* full-length substrates as well as the *UbInPD* peptide substrates we analyzed did not change in response to Ubiquilins or RAD23A/B ablation; thus, additional shuttling factors might be involved redundantly or in parallel to Ubiquilins and RAD23A/B members. For example, in the case of ODC, it has been demonstrated that the protein antizyme 1 (AZ1) accelerates its turnover by the 26S proteasome.[55]

Both 20S and 26S proteasomes can mediate proteolysis of *UbInPD* substrates

Two example *UbInPD* peptide substrates, ETV1 and FBXO6, were proteolyzed by both 20S and 26S proteasomes *in vitro*, while the *in vivo* degradation of *UbInPD* peptide substrates is mainly dependent on 26S proteasomes. One possible explanation for this discrepancy is that while under *in vitro* assay conditions the 20S is fully activated, 20S proteasomes *in vivo* are mostly present in a latent, autoinhibited state.[56–59] The fact that C23mers are proteolyzed *in vitro* when incubated with proteasomes suggests that C-degrons can directly promote substrate association with the proteasome. Similarly, the ODC degron was able to promote interaction with proteasomes in purified systems. However, ODC degradation is significantly slower *in vitro* unless AZ1 is added, suggesting a role for AZ1 in ODC unfolding following engagement.[8] Analogous factors yet-to-be-identified might promote more rapid elimination of the tested C23mers *in vitro*. *In vivo*, however, we speculate that GFP-fused *UbInPD* peptide substrates may be degraded even before they fully fold, arguing against the involvement of additional factors.

Ubiquitination-independent and -dependent mechanisms act in parallel to tightly control protein levels

Most of the known full-length *UbInPD* substrates can be targeted to the proteasome via both ubiquitin-dependent and independent mechanisms.[18,19] Indeed, we found for the full-length *UbInPD* substrates that we identified, mutation of the C terminus did not significantly change their stability, but rather converted their mode of degradation from ubiquitin-independent to ubiquitin-dependent. A similar phenomenon has been reported for RPN4, which is degraded via two independent mechanisms: one mechanism is dependent on an internal degron that leads to ubiquitination, whereas the other is mediated by an N-degron that is independent of ubiquitination. The fact that in most cases the overall stability of the wild-type and mutant substrates remain the same suggests that there is a tight control over their turnover, thus ensuring their degradation even if one pathway is inhibited.

BTG2, CDCA4, and REC8 were identified in our ORFeome screen as full-length proteins subjected to *UbInPD*. BTG2 functions as a transcriptional coactivator and was demonstrated to be a short-lived protein that is degraded in the proteasome in a ubiquitination-dependent manner.[60–62] Thus, *UbInPD* might be another regulatory mechanism to ensure tight control of its expression when the UPS is inhibited. As for CDCA4 and REC8, little is known about their mechanism of degradation. CDCA4 regulates cell proliferation[63] as well as cell death,[64] while REC8 has been shown to regulate viability and proliferation in thyroid and gastric cancers.[65,66] Thus, better understanding of the biological significance of *UbInPD* of CDCA4 and REC8 to their regulation and cellular function could have implications for diseases such as cancer.

Evolution of C-degron-mediated degradation from prokaryotes to eukaryotes

The utilization of C-degrons and adaptor proteins in promoting substrate degradation is conserved from bacteria to humans. In *E. coli* the small stable RNA A (ssrA) tag (AANDENYALAA) serves as a C-degron for the ClpXP and ClpAP proteasome-like proteases.[67] Similar to proteasomal Ala-end C-degron identified here, the terminal -AA dipeptide of ssrA degron is the most important element for ClpXP degradation,[68] and related C-degrons ending in alanine target other bacterial proteins to ClpXP.[69] These residues can directly associate with the ATPase ClpX to promote degradation,[70] although proteolysis is enhanced by the adaptor protein SspB.[71] While hydrophobic

residues were also proposed to function as C-degrons in bacteria,[72,73] whether additional classes of prokaryotic C-degrons and adaptor proteins exist is still an open question.

Similar to bacteria, archaeal C-degrons can also promote proteolysis. C-terminal hydrophobic tails in that case could stimulate the degradation of GFP by archaeal proteasomes *in vitro* via interaction with the proteasome-activating ATPase, proteasome-activating nucleotidase (PAN) regulatory complex.[74] We thus hypothesize that eukaryotic proteasomal degradation of C-terminal hydrophobic degrons fused to GFP (and potentially other GFP-fused C-degrons identified here) might be promoted by direct interaction with the eukaryotic proteasomal ATPase, although we cannot exclude the involvement of other subunits located in the 19S regulatory particle. Indeed, our *in vitro* assays with purified proteasomes showed that the hydrophobic *UbInPD* C-degrons of both model peptides (ETV1: -YVY*; FBXO6: -VVQIF*) could promote proteolysis of the GFP-fusions. *In vivo*, however, our understanding of the molecular mechanisms regulating substrate selection by proteasomes remains rudimentary, and future work is needed to investigate whether eukaryotic cellular factors similar to the bacterial adaptor protein SspB also play a stimulatory role. Overall, a better understanding of degrons involved in ubiquitin-independent targeting to eukaryotic proteasomes may shed light on conservation and evolution of protein degradation mechanisms across the three kingdoms of life.

Limitations of the study

While *in vitro* both 20S and 26S proteasomes can degrade GFP-fused peptides, *in vivo*, it is mostly done by 26S. Thus, 20S might be fully activated upon purification for *in vitro* assays and hence may not represent its latent state observed in cells. Even then, the relatively slow kinetics of GFP-fusions proteolysis observed *in vitro* compared with their rapid turnover detected *in vivo* suggests that although direct targeting of peptides to the proteasomes could occur, it cannot fully explain the mode of proteasomal targeting *in vivo*. Alternatively, other cellular factors that are missing in the *in vitro* reaction may also be required. The lack of involvement of UBA6 in the degradation of UBA1-independent substrates was ruled out based on a few examples of GFP-peptide reporters, and thus we cannot exclude that a minority of substrates that are not stabilized by MLN7243 treatment are targeted for destruction by UBA6. As effective commercial antibodies were not available to full-length *UbInPD* substrates, we could not investigate the molecular mechanism of proteasomal targeting and degradation at the endogenous level.

STAR★METHODS

Detailed methods are provided in the online version of this paper and include the following:

- KEY RESOURCES TABLE
- RESOURCE AVAILABILITY
  - Lead contact
  - Materials availability
  - Data and code availability
- EXPERIMENTAL MODEL AND SUBJECT DETAILS
  - Cell Lines
- METHOD DETAILS
  - Transfection and lentivirus production
  - Inhibitors
  - Plasmids
  - Generation of CRISPR-Cas9 knockout cells
  - Flow cytometry
  - Immunoblotting
  - Immunoprecipitation
  - Analysis of ubiquitination
  - Protein expression and purification
  - *In vitro* degradation assay with purified proteasomes
  - Rescue experiment with UBQLN1 cDNA
  - Microscopy
  - Generation of GPS-peptides libraries
  - GPS screens
- QUANTIFICATION AND STATISTICAL ANALYSIS
  - Analysis of GPS-C23mer screen
  - Analysis of GPS-ORFeome screen
  - Analysis of mutagenesis GPS-C23mer screens
  - Analysis of Disorder tendency
  - Statistical analysis of the distribution of PSI scores for all *UbInPD* peptides harboring specific C-terminal motifs
  - Quantification of *in vitro* degradation assays

SUPPLEMENTAL INFORMATION

Supplemental information can be found online at https://doi.org/10.1016/j.molcel.2023.04.023.

ACKNOWLEDGMENTS

We thank J. Adler (Y. Shaul lab, Weizmann Institute of Science) for providing PSMD1 and luciferase shRNAs, I. Sahu for help in purifying proteasomes, and M. Sharon (Weizmann Institute of Science) for providing pET28 vector. We are grateful to H. Hauschner for FACS. I.K. is supported by European Research Council (ERC-2020-STG 947709), Israel Science Foundation (ISF grants no. 2380/21 and 3096/21), Alon Fellowship, and The Applebaum Foundation. M.H.G. is funded by ISF 755/19, NSFC-ISF 2512/18 and a Russell Berrie Nanotechnology NEVET grant to A.R.W. and M.H.G. S.J.E. is funded by NIH grant AG11085. S.J.E. is an investigator with the Howard Hughes Medical Institute. R.T.T. is the recipient of a Pemberton-Trinity Fellowship.

AUTHOR CONTRIBUTIONS

Conceptualization, S.J.E. and I.K.; supervision, I.K.; methodology, S.J.E. and I.K.; software, Y.M., A.R., M.I.G., S.B., R.T.T., and I.K.; formal analysis, Y.M., R.T.T., A.R.W., M.H.G., and I.K.; investigation, Y.M., A.R., R.T.T., A.R.W., A.B., J.G.-H., M.H.G., and I.K.; writing – original draft, Y.M. and I.K.; writing & editing, Y.M. and I.K.

DECLARATION OF INTERESTS

S.J.E. is a member of the *Molecular Cell* advisory board.

Received: August 8, 2022
Revised: March 13, 2023
Accepted: April 25, 2023
Published: May 17, 2023

REFERENCES

1. Kwon, Y.T., and Ciechanover, A. (2017). The ubiquitin code in the ubiquitin-proteasome system and autophagy. Trends Biochem. Sci. *42*, 873–886. https://doi.org/10.1016/j.tibs.2017.09.002.
2. Hershko, A., and Ciechanover, A. (1998). The ubiquitin system. Annu. Rev. Biochem. *67*, 425–479. https://doi.org/10.1146/annurev.biochem.67.1.425.
3. Schrader, E.K., Harstad, K.G., and Matouschek, A. (2009). Targeting proteins for degradation. Nat. Chem. Biol. *5*, 815–822. https://doi.org/10.1038/nchembio.250.
4. Pickart, C.M. (2001). Mechanisms underlying ubiquitination. Annu. Rev. Biochem. *70*, 503–533. https://doi.org/10.1146/annurev.biochem.70.1.503.
5. Zheng, N., and Shabek, N. (2017). Ubiquitin ligases: structure, function, and regulation. Annu. Rev. Biochem. *86*, 129–157. https://doi.org/10.1146/annurev-biochem-060815-014922.
6. Lucas, X., and Ciulli, A. (2017). Recognition of substrate degrons by E3 ubiquitin ligases and modulation by small-molecule mimicry strategies. Curr. Opin. Struct. Biol. *44*, 101–110. https://doi.org/10.1016/j.sbi.2016.12.015.
7. Varshavsky, A. (1991). Naming a targeting signal. Cell *64*, 13–15.
8. Zhang, M., Pickart, C.M., and Coffino, P. (2003). Determinants of proteasome recognition of ornithine decarboxylase, a ubiquitin-independent substrate. EMBO J. *22*, 1488–1496. https://doi.org/10.1093/emboj/cdg158.
9. Murakami, Y., Matsufuji, S., Kameji, T., Hayashi, S.I., Igarashi, K., Tamura, T., Tanaka, K., and Ichihara, A. (1992). Ornithine decarboxylase is degraded by the 26S proteasome without ubiquitination. Nature *360*, 597–599. https://doi.org/10.1038/360597a0.
10. Asher, G., and Shaul, Y. (2005). p53 proteasomal degradation: poly-ubiquitination is not the whole story. Cell Cycle *4*, 1015–1018. https://doi.org/10.4161/cc.4.8.1900.
11. Asher, G., Tsvetkov, P., Kahana, C., and Shaul, Y. (2005). A mechanism of ubiquitin-independent proteasomal degradation of the tumor suppressors p53 and p73. Genes Dev. *19*, 316–321. https://doi.org/10.1101/gad.319905.
12. Chen, X., Chi, Y., Bloecher, A., Aebersold, R., Clurman, B.E., and Roberts, J.M. (2004). N-acetylation and ubiquitin-independent proteasomal degradation of p21(Cip1). Mol. Cell *16*, 839–847. https://doi.org/10.1016/j.molcel.2004.11.011.
13. Chen, X., Barton, L.F., Chi, Y., Clurman, B.E., and Roberts, J.M. (2007). Ubiquitin-independent degradation of cell-cycle inhibitors by the REGγ proteasome. Mol. Cell *26*, 843–852. https://doi.org/10.1016/j.molcel.2007.05.022.
14. Li, X., Amazit, L., Long, W., Lonard, D.M., Monaco, J.J., and O'Malley, B.W. (2007). Ubiquitin- and ATP-independent proteolytic turnover of p21 by the REGgamma-proteasome pathway. Mol. Cell *26*, 831–842. https://doi.org/10.1016/j.molcel.2007.05.028.
15. Bossis, G., Ferrara, P., Acquaviva, C., Jariel-Encontre, I., and Piechaczyk, M. (2003). c-Fos Proto-Oncoprotein Is Degraded by the proteasome Independently of Its Own ubiquitinylation in vivo. Mol. Cell. Biol. *23*, 7425–7436. https://doi.org/10.1128/MCB.23.20.7425-7436.2003.
16. Bercovich, Z., Rosenberg-Hasson, Y., Ciechanover, A., and Kahana, C. (1989). Degradation of ornithine decarboxylase in reticulocyte lysate is ATP-dependent but ubiquitin-independent. J. Biol. Chem. *264*, 15949–15952. https://doi.org/10.1016/s0021-9258(18)71571-8.
17. Ju, D., and Xie, Y. (2004). Proteasomal degradation of RPN4 via two distinct mechanisms, ubiquitin-dependent and -independent. J. Biol. Chem. *279*, 23851–23854. https://doi.org/10.1074/jbc.C400111200.
18. Erales, J., and Coffino, P. (2014). Ubiquitin-independent proteasomal degradation. Biochim. Biophys. Acta *1843*, 216–221. https://doi.org/10.1016/j.bbamcr.2013.05.008.
19. Jariel-Encontre, I., Bossis, G., and Piechaczyk, M. (2008). Ubiquitin-independent degradation of proteins by the proteasome. Biochim. Biophys. Acta *1786*, 153–177. https://doi.org/10.1016/j.bbcan.2008.05.004.
20. Miyazaki, Y., Matsufuji, S., Murakami, Y., and Hayashi, S. (1993). Single amino-acid replacement is responsible for the stabilization of ornithine decarboxylase in HMOA cells. Eur. J. Biochem. *214*, 837–844. https://doi.org/10.1111/j.1432-1033.1993.tb17987.x.
21. Li, X., Zhao, X., Fang, Y., Jiang, X., Duong, T., Fan, C., Huang, C.C., and Kain, S.R. (1998). Generation of destabilized green fluorescent protein as a transcription reporter. J. Biol. Chem. *273*, 34970–34975. https://doi.org/10.1074/jbc.273.52.34970.
22. Gandre, S., and Kahana, C. (2002). Degradation of ornithine decarboxylase in Saccharomyces cerevisiae is ubiquitin independent. Biochem. Biophys. Res. Commun. *293*, 139–144. https://doi.org/10.1016/S0006-291X(02)00194-8.
23. Kisselev, A.F., Kaganovich, D., and Goldberg, A.L. (2002). Binding of hydrophobic peptides to several non-catalytic sites promotes peptide hydrolysis by all active sites of 20 S proteasomes. Evidence for peptide-induced channel opening in the α-rings. J. Biol. Chem. *277*, 22260–22270. https://doi.org/10.1074/jbc.M112360200.
24. Touitou, R., Richardson, J., Bose, S., Nakanishi, M., Rivett, J., and Allday, M.J. (2001). A degradation signal located in the C-terminus of p21WAF1/CIP1 is a binding site for the C8 α-subunit of the 20S proteasome. EMBO J. *20*, 2367–2375. https://doi.org/10.1093/emboj/20.10.2367.
25. Koren, I., Timms, R.T., Kula, T., Xu, Q., Li, M.Z., and Elledge, S.J. (2018). The eukaryotic proteome is shaped by E3 ubiquitin ligases targeting C-terminal degrons. Cell *173*, 1622–1635.e14. https://doi.org/10.1016/j.cell.2018.04.028.
26. Timms, R.T., Zhang, Z., Rhee, D.Y., Harper, J.W., Koren, I., and Elledge, S.J. (2019). A glycine-specific N-degron pathway mediates the quality control of protein *N* -myristoylation. Science *365*, eaaw4912. https://doi.org/10.1126/science.aaw4912.
27. Yen, H.C., Xu, Q., Chou, D.M., Zhao, Z., and Elledge, S.J. (2008). Global protein stability profiling in mammalian cells. Science *322*, 918–923. https://doi.org/10.1126/science.1160489.
28. Hyer, M.L., Milhollen, M.A., Ciavarri, J., Fleming, P., Traore, T., Sappal, D., Huck, J., Shi, J., Gavin, J., Brownell, J., et al. (2018). A small-molecule inhibitor of the ubiquitin activating enzyme for cancer treatment. Nat. Med. *24*, 186–193. https://doi.org/10.1038/nm.4474.
29. Ravichandran, R., Kodali, K., Peng, J., and Potts, P.R. (2019). Regulation of MAGE-A3/6 by the CRL4- DCAF12 ubiquitin ligase and nutrient availability. EMBO Rep. *20*, e47352. https://doi.org/10.15252/embr.201847352.
30. Barker, D.F., and Campbell, A.M. (1981). The birA gene of Escherichia coli encodes a biotin holoenzyme synthetase. J. Mol. Biol. *146*, 451–467. https://doi.org/10.1016/0022-2836(81)90042-5.
31. Jin, J., Li, X., Gygi, S.P., and Harper, J.W. (2007). Dual E1 activation systems for ubiquitin differentially regulate E2 enzyme charging. Nature *447*, 1135–1138. https://doi.org/10.1038/nature05902.
32. Fredrickson, E.K., Rosenbaum, J.C., Locke, M.N., Milac, T.I., and Gardner, R.G. (2011). Exposed hydrophobicity is a key determinant of nuclear quality control degradation. Mol. Biol. Cell *22*, 2384–2395. https://doi.org/10.1091/mbc.E11-03-0256.
33. Sahu, I., Mali, S.M., Sulkshane, P., Xu, C., Rozenberg, A., Morag, R., Sahoo, M.P., Singh, S.K., Ding, Z., Wang, Y., et al. (2021). The 20S as a stand-alone proteasome in cells can degrade the ubiquitin tag. Nat. Commun. *12*, 6173. https://doi.org/10.1038/s41467-021-26427-0.
34. Berko, D., Tabachnick-Cherny, S., Shental-Bechor, D., Cascio, P., Mioletti, S., Levy, Y., Admon, A., Ziv, T., Tirosh, B., Goldberg, A.L., et al. (2012). The direction of protein entry into the proteasome determines the variety of products and depends on the force needed to unfold its two termini. Mol. Cell *48*, 601–611. https://doi.org/10.1016/j.molcel.2012.08.029.
35. Tsvetkov, P., Adler, J., Myers, N., Biran, A., Reuven, N., and Shaul, Y. (2018). Oncogenic addiction to high 26S proteasome level. Cell Death Dis. *9*, 773. https://doi.org/10.1038/s41419-018-0806-4.
36. Basbous, J., Jariel-Encontre, I., Gomard, T., Bossis, G., and Piechaczyk, M. (2008). Ubiquitin-independent- versus ubiquitin-dependent proteasomal

degradation of the c-Fos and Fra-1 transcription factors: is there a unique answer? Biochimie *90*, 296–305. https://doi.org/10.1016/j.biochi.2007.07.016.

37. Jantrapirom, S., Piccolo, L. lo, and Yamaguchi, M. (2019). Non-proteasomal UbL-UbA family of proteins in neurodegeneration. Int. J. Mol. Sci. *20*. https://doi.org/10.3390/ijms20081893.
38. Huang, D.W., Sherman, B.T., and Lempicki, R.A. (2009). Systematic and integrative analysis of large gene lists using David bioinformatics resources. Nat. Protoc. *4*, 44–57. https://doi.org/10.1038/nprot.2008.211.
39. Huang, D.W., Sherman, B.T., and Lempicki, R.A. (2009). Bioinformatics enrichment tools: paths toward the comprehensive functional analysis of large gene lists. Nucleic Acids Res. *37*, 1–13. https://doi.org/10.1093/nar/gkn923.
40. Dosztányi, Z., Csizmok, V., Tompa, P., and Simon, I. (2005). IUPred: web server for the prediction of intrinsically unstructured regions of proteins based on estimated energy content. Bioinformatics *21*, 3433–3434. https://doi.org/10.1093/bioinformatics/bti541.
41. Li, C., Franklin, J.L., Graves-Deal, R., Jerome, W.G., Cao, Z., and Coffey, R.J. (2004). Myristoylated Naked2 escorts transforming growth factor α to the basolateral plasma membrane of polarized epithelial cells. Proc. Natl. Acad. Sci. USA *101*, 5571–5576. https://doi.org/10.1073/pnas.0401294101.
42. Yu, H., and Matouschek, A. (2017). Recognition of client proteins by the proteasome. Annu. Rev. Biophys. *46*, 149–173. https://doi.org/10.1146/annurev-biophys-070816-033719.
43. Zientara-Rytter, K., and Subramani, S. (2019). The roles of ubiquitin-binding protein shuttles in the degradative fate of ubiquitinated proteins in the ubiquitin-proteasome system and autophagy. Cells *8*. https://doi.org/10.3390/cells8010040.
44. MacLean, A.M., Orlovskis, Z., Kowitwanich, K., Zdziarska, A.M., Angenent, G.C., Immink, R.G.H., and Hogenhout, S.A. (2014). Phytoplasma effector SAP54 hijacks plant reproduction by degrading MADS-box proteins and promotes insect colonization in a RAD23-dependent manner. PLoS Biol. *12*, e1001835. https://doi.org/10.1371/journal.pbio.1001835.
45. Huang, W., MacLean, A.M., Sugio, A., Maqbool, A., Busscher, M., Cho, S.T., Kamoun, S., Kuo, C.H., Immink, R.G.H., and Hogenhout, S.A. (2021). Parasitic modulation of host development by ubiquitin-independent protein degradation. Cell *184*, 5201–5214.e12. https://doi.org/10.1016/j.cell.2021.08.029.
46. Zhao, G., Zhou, X., Wang, L., Li, G., Kisker, C., Lennarz, W.J., and Schindelin, H. (2006). Structure of the mouse peptide N-glycanase-HR23 complex suggests co-evolution of the endoplasmic reticulum-associated degradation and DNA repair pathways. J. Biol. Chem. *281*, 13751–13761. https://doi.org/10.1074/jbc.M600137200.
47. Stieren, E.S., el Ayadi, A., Xiao, Y., Siller, E., Landsverk, M.L., Oberhauser, A.F., Barral, J.M., and Boehning, D. (2011). Ubiquilin-1 is a molecular chaperone for the amyloid precursor protein. J. Biol. Chem. *286*, 35689–35698. https://doi.org/10.1074/jbc.M111.243147.
48. Itakura, E., Zavodszky, E., Shao, S., Wohlever, M.L., Keenan, R.J., and Hegde, R.S. (2016). Ubiquilins chaperone and triage mitochondrial membrane proteins for degradation. Mol. Cell *63*, 21–33. https://doi.org/10.1016/j.molcel.2016.05.020.
49. Kurlawala, Z., Shah, P.P., Shah, C., and Beverly, L.J. (2017). The STI and UBA domains of UBQLN1 are critical determinants of substrate interaction and proteostasis. J. Cell. Biochem. *118*, 2261–2270. https://doi.org/10.1002/jcb.25880.
50. Baugh, J.M., Viktorova, E.G., and Pilipenko, E.V. (2009). Proteasomes can degrade a significant proportion of cellular proteins independent of ubiquitination. J. Mol. Biol. *386*, 814–827. https://doi.org/10.1016/j.jmb.2008.12.081.
51. Hegde, R.S., and Zavodszky, E. (2019). Recognition and degradation of mislocalized proteins in health and disease. Cold Spring Harb. Perspect. Biol. *11*, a033902. https://doi.org/10.1101/cshperspect.a033902.
52. Hessa, T., Sharma, A., Mariappan, M., Eshleman, H.D., Gutierrez, E., and Hegde, R.S. (2011). Protein targeting and degradation are coupled for elimination of mislocalized proteins. Nature *475*, 394–397. https://doi.org/10.1038/nature10181.
53. Rodrigo-Brenni, M.C., Gutierrez, E., and Hegde, R.S. (2014). Cytosolic quality control of mislocalized proteins requires RNF126 recruitment to Bag6. Mol. Cell *55*, 227–237. https://doi.org/10.1016/j.molcel.2014.05.025.
54. Suzuki, R., and Kawahara, H. (2016). UBQLN4 recognizes mislocalized transmembrane domain proteins and targets these to proteasomal degradation. EMBO Rep. *17*, 842–857. https://doi.org/10.15252/embr.201541402.
55. Li, X., and Coffino, P. (1992). Regulated degradation of ornithine decarboxylase requires interaction with the polyamine-inducible protein antizyme. Mol. Cell. Biol. *12*, 3556–3562. https://doi.org/10.1128/mcb.12.8.3556-3562.1992.
56. Groll, M., Bajorek, M., Köhler, A., Moroder, L., Rubin, D.M., Huber, R., Glickman, M.H., and Finley, D. (2000). A gated channel into the proteasome core particle. Nat. Struct. Biol. *7*, 1062–1067. https://doi.org/10.1038/80992.
57. Köhler, A., Cascio, P., Leggett, D.S., Woo, K.M., Goldberg, A.L., and Finley, D. (2001). The axial channel of the proteasome core particle is gated by the Rpt2 ATPase and controls both substrate entry and product release. Mol. Cell *7*, 1143–1152. https://doi.org/10.1016/S1097-2765(01)00274-X.
58. Coux, O., Tanaka, K., and Goldberg, A.L. (1996). Structure and functions of the 20s AND 26s proteasomes. Annu. Rev. Biochem. *65*, 801–847.
59. McGuire, M.J., McCullough, M.L., Croall, D.E., and DeMartino, G.N. (1989). The high molecular weight multicatalytic proteinase, macropain, exists in a latent form in human erythrocytes. Biochim. Biophys. Acta *995*, 181–186. https://doi.org/10.1016/0167-4838(89)90078-2.
60. Park, T.J., Kim, J.Y., Park, S.H., Kim, H.S., and Lim, I.K. (2009). Skp2 enhances polyubiquitination and degradation of TIS21/BTG2/PC3, tumor suppressor protein, at the downstream of FoxM1. Exp. Cell Res. *315*, 3152–3162. https://doi.org/10.1016/j.yexcr.2009.07.009.
61. Sasajima, H., Nakagawa, K., Kashiwayanagi, M., and Yokosawa, H. (2012). Polyubiquitination of the B-cell translocation gene 1 and 2 proteins is promoted by the SCF ubiquitin ligase complex containing βTrCP. Biol. Pharm. Bull. *35*, 1539–1545. https://doi.org/10.1248/bpb.b12-00330.
62. Sasajima, H., Nakagawa, K., and Yokosawa, H. (2002). Antiproliferative proteins of the BTG/Tob family are degraded by the ubiquitin-proteasome system. Eur. J. Biochem. *269*, 3596–3604. https://doi.org/10.1046/j.1432-1033.2002.03052.x.
63. Hayashi, R., Goto, Y., Ikeda, R., Yokoyama, K.K., and Yoshida, K. (2006). CDCA4 is an E2F transcription factor family-induced nuclear factor that regulates E2F-dependent transcriptional activation and cell proliferation. J. Biol. Chem. *281*, 35633–35648. https://doi.org/10.1074/jbc.M603800200.
64. Li, C., Jung, S., Lee, S., Jeong, D., Yang, Y., Kim, K. il, Lim, J.S., Cheon, C. il, Kim, C., Kang, Y.S., and Lee, M.-S. (2015). Nutrient/serum starvation derived TRIP-Br3 down-regulation accelerates apoptosis by destabilizing XIAP. Oncotarget *6*, 7522–7535. https://doi.org/10.18632/oncotarget.3112.
65. Liu, D., Shen, X., Zhu, G., and Xing, M. (2015). REC8 is a novel tumor suppressor gene epigenetically robustly targeted by the PI3K pathway in thyroid cancer. Oncotarget *6*, 39211–39224. https://doi.org/10.18632/oncotarget.5391.
66. Yu, J., Liang, Q., Wang, J., Wang, K., Gao, J., Zhang, J., Zeng, Y., Chiu, P.W.Y., Ng, E.K.W., and Sung, J.J.Y. (2017). REC8 functions as a tumor suppressor and is epigenetically downregulated in gastric cancer, especially in EBV-positive subtype. Oncogene *36*, 182–193. https://doi.org/10.1038/onc.2016.187.
67. Gottesman, S., Roche, E., Zhou, Y., and Sauer, R.T. (1998). The ClpXP and ClpAP proteases degrade proteins with carboxy-terminal peptide tails added by the SsrA-tagging system. Genes Dev. *12*, 1338–1347. https://doi.org/10.1101/gad.12.9.1338.

68. Flynn, J.M., Levchenko, I., Seidel, M., Wickner, S.H., Sauer, R.T., and Baker, T.A. (2001). Overlapping recognition determinants within the ssrA degradation tag allow modulation of proteolysis. Proc. Natl. Acad. Sci. USA *98*, 10584–10589. https://doi.org/10.1073/pnas.191375298.

69. Flynn, J.M., Neher, S.B., Kim, Y.I., Sauer, R.T., and Baker, T.A. (2003). Proteomic discovery of cellular substrates of the ClpXP protease reveals five classes of ClpX-recognition signals. Mol. Cell *11*, 671–683. https://doi.org/10.1016/S1097-2765(03)00060-1.

70. Fei, X., Bell, T.A., Barkow, S.R., Baker, T.A., and Sauer, R.T. (2020). Structural basis of ClpXP recognition and unfolding of ssrA-tagged substrates. eLife *9*. https://doi.org/10.7554/eLife.61496.

71. Levchenko, I., Seidel, M., Sauer, R.T., and Baker, T.A. (2000). A specificity-enhancing factor for the ClpXP degradation machine. Science *289*, 2354–2356. https://doi.org/10.1126/science.289.5488.2354.

72. Parsell, D.A., Silber, K.R., and Sauer, R.T. (1990). Carboxy-terminal determinants of intracellular protein degradation. Genes Dev. *4*, 277–286. https://doi.org/10.1101/gad.4.2.277.

73. Weber, M., Burgos, R., Yus, E., Yang, J.S., Lluch-Senar, M., and Serrano, L. (2020). Impact of C-terminal amino acid composition on protein expression in bacteria. Mol. Syst. Biol. *16*, e9208. https://doi.org/10.15252/msb.20199208.

74. Benaroudj, N., Zwickl, P., Seemüller, E., Baumeister, W., and Goldberg, A.L. (2003). ATP hydrolysis by the proteasome regulatory complex PAN serves multiple functions in protein degradation. Mol. Cell *11*, 69–78. https://doi.org/10.1016/S1097-2765(02)00775-X.

75. Unk, I., Hajdú, I., Fátyol, K., Hurwitz, J., Yoon, J.H., Prakash, L., Prakash, S., and Haracska, L. (2008). Human HLTF functions as a ubiquitin ligase for proliferating cell nuclear antigen polyubiquitination. Proc. Natl. Acad. Sci. USA *105*, 3768–3773. https://doi.org/10.1073/pnas.0800563105.

76. Martin, M. (2011). Cutadapt removes adapter sequences from high-throughput sequencing reads. EMBnet J *17*, 10–12. https://doi.org/10.14806/ej.17.1.200.

77. Langmead, B., and Salzberg, S.L. (2012). Fast gapped-read alignment with Bowtie 2. Nat. Methods *9*, 357–359. https://doi.org/10.1038/nmeth.1923.

78. Langmead, B., Trapnell, C., Pop, M., and Salzberg, S.L. (2009). Ultrafast and memory-efficient alignment of short DNA sequences to the human genome. Genome Biol. *10*, R25. https://doi.org/10.1186/gb-2009-10-3-r25.

79. Schneider, C.A., Rasband, W.S., and Eliceiri, K.W. (2012). NIH Image to ImageJ: 25 years of image analysis. Nat. Methods *9*, 671–675. https://doi.org/10.1038/nmeth.2089.

80. Sanjana, N.E., Shalem, O., and Zhang, F. (2014). Improved vectors and genome-wide libraries for CRISPR screening. Nat. Methods *11*, 783–784. https://doi.org/10.1038/nmeth.3047.

81. Erdős, G., and Dosztányi, Z. (2020). Analyzing protein disorder with IUPred2A. Curr. Protoc. Bioinformatics *70*, e99. https://doi.org/10.1002/cpbi.99.

STAR★METHODS

KEY RESOURCES TABLE

REAGENT or RESOURCE	SOURCE	IDENTIFIER
Antibodies		
Mouse anti-Vinculin	Sigma-Aldrich	Cat# V9131; RRID: AB_477629
Rabbit Anti-NRF2 (D1Z9C) XP	Cell Signaling Technology	Cat# 12721; RRID: AB_2715528
Rabbit anti-HSP70	Cell Signaling Technology	Cat# 4873; RRID: AB_2119694
Rabbit anti-HA	Cell Signaling Technology	Cat# 3724; RRID: AB_1549585
Rabbit anti-TSPYL1	Abcam	Cat# ab95943; RRID: AB_10678086
Rabbit anti-GFP	Abcam	Cat# ab290; RRID: AB_303395
Rabbit anti-CCT5	Bethyl Laboratories	Cat# A303-480A; RRID: AB_10954003
Rabbit anti-UBA6	Bethyl Laboratories	Cat# A304-106A; RRID: AB_2621355
Rabbit anti-HIF1α	Bethyl Laboratories	Cat# A300-286A; RRID: AB_2117114
Mono- and polyubiquitinylated conjugates monoclonal antibody (FK2) (HRP conjugate)	Enzo Life Sciences	Cat# BML-PW0150-0100; RRID: N/A
Mouse anti-Ubiquitin Antibody	LifeSensors	Cat# VU101; RRID: AB_2716558
Mouse anti-GST (B-14)	Santa Cruz Biotechnology	Cat# sc-138; RRID: AB_627677
Goat Anti-Rabbit IgG (H+L) HRP	Jackson ImmunoResearch Labs	Cat# 111-035-003; RRID: AB_2313567
Goat Anti-Mouse IgG (H+L) HRP	Jackson ImmunoResearch Labs	Cat# 115-035-003; RRID: AB_10015289
Bacterial and virus strains		
E. coli DH5alpha	New England Biolabs	Cat# C2527I
E. coli ElectroMAX DH10β	Thermo Fisher Scientific	Cat# 18290015
Tuner™(DE3) Competent Cells – Novagen	Sigma-Aldrich	Cat# 70623
E. coli BL21 (DE3) cells	This paper	N/A
Chemicals, peptides, and recombinant proteins		
Bortezomib	APExBio	Cat# A2614
MLN7243 (TAK-243)	Selleck Chemicals	Cat# S8341
Polybrene	Santa Cruz Biotechnology	Cat# sc-134220
PolyJet In Vitro DNA Transfection Reagent	SignaGen	Cat# SL100688
PR-619	EMD Millipore	Cat# 662141
Critical commercial assays		
Q5® Hot Start High-Fidelity DNA Polymerase	New England Biolabs	Cat# M0493S
QIAEX II Gel Extraction Kit	QIAGEN	Cat# 20051
PCR purification kit	QIAGEN	Cat# 28106
Gentra Puregene Cell Kit	QIAGEN	Cat# 158767
Direct-zol RNA Microprep Kits	Zymo Research	Cat# R2061
qScript cDNA Synthesis Kit	Quantabio	Cat# 95047-025
ChromoTek GFP-Trap® Magnetic Agarose	Proteintech	Cat# gtma
Gateway™ BP Clonase™ II Enzyme mix	Thermo Fisher Scientific	Cat# 11789020
Gateway™ LR Clonase™ II Enzyme mix	Thermo Fisher Scientific	Cat# 11791020
Experimental models: Cell lines		
HEK293T	ATCC	ATCC® CRL-3216™
U2OS	Dr. Yaron Shav-Tal	N/A
mIMCD-3 cells	Dr. Achia Urbach	N/A
Oligonucleotides		
sg1-UBA6: GTATGTGATGAGGACGAAAT	This paper	N/A
sg2-UBA6: GCCTGTGGCCGCCCATCAGG	This paper	N/A

(*Continued on next page*)

Continued

REAGENT or RESOURCE	SOURCE	IDENTIFIER
sg-UBQLN1: GCGAGAATAGCTCCGTCCAGC	This paper	N/A
sg-UBQLN2: GCGCGGGAACTAACACTACCT	This paper	N/A
sg-UBQLN4: GCTCTTGATCACAGTTCAAAG	This paper	N/A
sg-RAD23A: GAAGGATGTAGAGGACTCTG	This paper	N/A
sg-RAD23B: GTAACTGCTGTAGTGCTGGC	This paper	N/A
sg-AAVSI: GGGGCCACTAGGGACAGGAT	Koren et al.[25]	N/A
Oligonucleotide Libraries listed in Tables S1 and S2	Agilent	N/A
Recombinant DNA		
pHAGE-GPS3.0-DEST	Koren et al.[25]	N/A
Barcoded GPS-ORFeome expression library	Koren et al.[25]	N/A
pHAGE-GPS3.0-peptide libraries	Koren et al.[25]	N/A
pHAGE-Flag-HA-DEST	Koren et al.[25]	N/A
pHAGE-ORF-IRES-BFP	This paper	N/A
pRK5-HA-Ubiquitin-WT	Addgene	Cat# 17608
pRK5-HA-Ubiquitin-K0	Addgene	Cat# 17603
pIL1377-HA-Ubiquitin	Unk et al.[75]	N/A
lentiCRISPR v2	Addgene	Cat# 52961
GST-Cyclin-B1-NT	This paper	N/A
pET28 N-terminal Hisx6-tag-GFP-peptide	This paper	N/A
pHAGE-EF1α-BirA-pep-PGK-Crimson	This paper	N/A
Software and algorithms		
Cutadapt	Martin[76]	http://cutadapt.readthedocs.io/en/stable/index.html
Bowtie 2	Langmead and Salzberg[77]; Langmead et al.[78]	http://bowtie-bio.sourceforge.net/index.shtml
Seaborn visualization library for Python	Seaborn	https://seaborn.pydata.org/
Flojow	Flojow	https://www.flowjo.com
ICE Analysis tool v3	Synthego	https://ice.synthego.com/#/
ImageJ software	NIH[79]	https://imagej.nih.gov/ij/download.html
Graphpad Prism V9 software	GraphPad Software	https://www.graphpad.com/scientific-software/prism/

RESOURCE AVAILABILITY

Lead contact

Further information and requests for resources and reagents should be directed to and will be fulfilled by the lead contact, Itay Koren (itay.koren@biu.ac.il).

Materials availability

Any reagents that are unique to this study will be made available upon request.

Data and code availability

- All data generated and analyzed during this study are included in this manuscript and the Supplementary Data.
- This paper does not report original code.
- Any additional information required to reanalyze the data reported in this paper is available from the lead contact upon request.

EXPERIMENTAL MODEL AND SUBJECT DETAILS

Cell Lines

HEK293T (ATCC® CRL-3216™), U2OS (A gift from Y. Shav-Tal lab, Bar-Ilan University) and mIMCD-3 cells (A gift from A. Urbach lab, Bar-Ilan University) were grown in Dulbecco's Modified Eagle's Medium (DMEM) (Life Technologies) supplemented with 10% fetal

bovine serum (Gibco) and penicillin/streptomycin (Life Technologies). HEK293T sh-Luciferase and sh-PSMD1 cells obtained from Y. Shaul lab (Weizmann Institute of Science).[35]

METHOD DETAILS

Transfection and lentivirus production

Lentivirus was generated through the transfection of HEK293T cells using PolyJet In Vitro DNA Transfection Reagent (SignaGen Laboratories). Cells seeded at approximately 80% confluency were transfected as recommended by the manufacturer with the lentiviral transfer vector plus four plasmids encoding Gag-Pol, Rev, Tat and VSV-G. The media was changed 24 h post-transfection and lentiviral supernatants collected a further 24 h later. Cell debris was removed by centrifugation (800 x *g*, 5 min) and virus was stored in single-use aliquots at -80°C. Transduction of target cells was achieved by adding the virus in the presence of 8 μg/ml hexadimethrine bromide (Polybrene).

Inhibitors

The proteasome inhibitor Bortezomib and the E1 inhibitor MLN7243 were used at a final concentration of 1 μM unless otherwise indicated.

Plasmids

ORFs encoding ABCC5, NKD2, BTG2, CDCA4, REC8, LRRN4CL, UBQLNL, GRID1, NNAT, PYCRL and RBM38 were obtained in the form of entry clones from the Ultimate ORF Clone collection (Thermo Fisher Scientific). UBQLN1 ORF was obtained by PCR reaction done on a cDNA library synthesized from HEK293T. To monitor stability by flow cytometry, ORFs were amplified by PCR to include BstBI and XhoI sites and were cloned by ligation into pHAGE-GPS3.0-DEST. To monitor ORFs levels by western blot, ORFs were amplified by PCR to include an HA epitope at their N terminus and subcloned into the lentiviral pHAGE vector that also contains IRES BFP cassette to monitor equal expression of the various constructs by flow cytometry. Peptides used in this study were encoded as oligonucleotides (gBlocks Gene Fragments, Integrated DNA Technologies (IDT)) and cloned into the pHAGE-GPS3.0 vector using the BstBI and XhoI sites. Sequences of all peptides appears in Table S1. The 19mer peptide named 'LSS' (peptide #2 from Fredrickson et al.[32]) amino acid sequence is: LSSNVYRAPLFVFVLYIII*. FBXO6 (QPGQRHGQEEAAQSPYRAVVQIF*) and ETV1 (ESMAYMPEGGCCNPHPYNEGYVY*) C23mers used as K_0BirA fusions do not encode lysine residues. BirA (WT and K_0BirA) were synthesized as gBlock by IDT, and cloned into pHAGE vector with or without fused peptides, under EF1α promoter. The pHAGE vector also encodes for Crimson under PGK promoter to enable the control of equal expression of the various BirA-fusions. pIL1377 plasmid encoding HA-Ubiquitin used in Figures 4A–4C was obtained from Haracska L. lab.[75] pRK5-HA-Ubiquitin-WT (#17608) and pRK5-HA-Ubiquitin-K0 (#17603) were obtained from Addgene and were used in Figures 4D, 6B, and S4B.

For individual CRISPR-Cas9-mediated gene disruption experiments, the lentiCRISPR v2 vector was used (Addgene #52961). Oligonucleotides encoding the top and bottom strands of the sgRNAs were synthesized (IDT), annealed and cloned into the lentiCRISPR v2 vector as described.[80]

Nucleotide sequences of the sgRNAs used were:
sg-AAVSI: GGGGCCACTAGGGACAGGAT
sg1-UBA6: GTATGTGATGAGGACGAAAT
sg2-UBA6: GCCTGTGGCCGCCCATCAGG
sg-UBQLN1: GCGAGAATAGCTCCGTCCAGC
sg-UBQLN2: GCGCGGGAACTAACACTACCT
sg-UBQLN4: GCTCTTGATCACAGTTCAAAG
sg-RAD23A: GAAGGATGTAGAGGACTCTG
sg-RAD23B: GTAACTGCTGTAGTGCTGGC

Generation of CRISPR-Cas9 knockout cells

Lentivirus was generated through the transfection of HEK293T with lentiCRISPR v2 as explained before. For generation of UBA6 KO cells, the two UBA6 sgRNAs were used simultaneously to transduce HEK293T cells. 48 h following transduction cells were selected with puromycin to eliminate non transduced cells. Ubiquilins triple KO cells were generated by simultaneously transduction of sgRNAs for UBQLN1, UBQLN2 and UBQLN4. RAD23 double KO cells were generated by simultaneously transduction of sgRNAs for RAD23A and RAD23B. Ubiquilins/RAD23 penta KO cells were generated by simultaneous transduction of Ubiquilins triple KO cells with RAD23A/B sgRNAs. 7 days post transduction, genomic DNA of transduced cells was extracted, PCRs were performed to amplify ~500 base pairs flanking the edited site followed by Sanger sequencing. Inference of CRISPR Edits (ICE) CRISPR Analysis Tool was used to analyze efficiency of editing (Synthego Performance Analysis, ICE Analysis. 2019. v3.0.).

Flow cytometry

Analysis of HEK293T cells by flow cytometry was performed on a BD LSRII or LSRFortessa instruments (Becton Dickinson) or CytoFLEX (Beckman Coulter) and the resulting data was analyzed using FlowJo. Cell sorting was performed on a MoFlo Astrios (Beckman Coulter) or BD FACSAria™ II (Becton Dickinson).

Immunoblotting

Cells were lysed in ice-cold lysis buffer (10 mM $NaPO_4$, 100 mM NaCl, 5mM EDTA pH 8, 1% Triton X-100, 0.5% Deoxycholic acid sodium salt, 0.1% SDS) supplemented with Halt™ Protease and Phosphatase Inhibitor Cocktail (Thermo Scientific) for 25 min at 4°C. Lysates were clarified by centrifugation (20,000 x g, 15 min, 4°C) and nuclear pellets were resuspended in lysis buffer, sonicated briefly, and re-clarified. Protein concentration was determined by a standard Bradford assay (Bio-Rad #500-0006), a linear bovine serum albumin (BSA) calibration curve, and an Epoch microplate spectrophotometer. Proteins were subsequently resolved by SDS-PAGE (Mini-PROTEAN TGX Precast Protein Gels, Bio-Rad) and transferred to a nitrocellulose membrane (Trans-Blot Turbo System, Bio-Rad) which was then blocked in 10% nonfat dry milk in PBS + 0.1% Tween-20 (PBS-T). The membrane was incubated with primary antibody overnight at 4°C, and then, following three washes with PBS-T, HRP-conjugated secondary antibody was added for 1 h at room temperature. Following a further three washes in PBS-T, reactive bands were visualized using SuperSignal West Femtochemiluminescence substrate (Pierce; #34095) or an EZ-ECL (Biological Industries; #20-500-171) for 5 min. Reactive bands visualized using the ImageQuant TL software v8.2 on Amersham Imager 680 (Cytiva).

Immunoprecipitation

HEK293T cells stably expressing single copy integrants of HA-tagged UBQLN1 with or without GFP-fused ORFs *UbInPD* substrates were generated by lentiviral transduction. For immunoprecipitation, 10 cm plates were treated with 1 μM MLN7243 + 1 μM bortezomib for 5 h followed by lysis in ice-cold lysis buffer (10 mM $NaPO_4$, 100 mM NaCl, 5mM EDTA pH 8, 1% Triton X-100, 0.5% Deoxycholic acid sodium salt, 0.1% SDS) supplemented with Halt™ Protease and Phosphatase Inhibitor Cocktail (Thermo Scientific) for 25 min at 4°C. Lysates were clarified by centrifugation (20,000 x g, 15 min, 4°C) followed by immunoprecipitation using GFP-Trap_MA magnetic agarose beads (Chromotek) that were added to the supernatants and incubated with rotation for 1 h at 4°C. The beads were then washed three times with lysis buffer before bound proteins were eluted upon incubation with SDS-PAGE sample buffer (95°C, 10 min). Proteins were subsequently resolved by SDS-PAGE as explained before.

Analysis of ubiquitination

HEK293T cells stably expressing GFP-peptide fusions were grown in 10 cm plates and transfected with HA-ubiquitin. 48 h post transfection, cells were treated with bortezomib (1 μM, 5 h), and then were lysed in ice-cold lysis buffer (10 mM $NaPO_4$, 100mM NaCl, 5mM EDTA pH 8, 1% Triton X-100, 0.5% Deoxycholic acid sodium salt, 0.1% SDS) supplemented with Halt™ Protease and Phosphatase Inhibitor Cocktail (Thermo Scientific) and 50 μM of the de-ubiquitinating enzyme inhibitor PR-619 for 30 min on ice. Nuclei were pelleted by centrifugation (14,000 x *g*, 10 min, 4°C). Protein concentration was determined by Bradford assay and equal amounts were taken for immunoprecipitation experiment by incubation for 1 h with 20 μl GFP-Trap_MA magnetic agarose beads . The beads were then stringently washed three times using wash buffer (10 mM $NaPO_4$, 300 mM NaCl, 5mM EDTA pH 8, 1% Triton X-100, 0.5% Deoxycholic acid sodium salt, 0.1% SDS) supplemented with Halt™ Protease and Phosphatase Inhibitor Cocktail and 50 μM PR-619 before bound proteins were eluted upon incubation with SDS-PAGE sample buffer (95°C, 10 min). SDS-PAGE and immunoblot was done as explained before.

Protein expression and purification

GFP and GFP-fused ETV1 and FBXO6 C23mers were cloned into pET28 vector which includes an amino-terminal Hisx6-tag. The constructs were expressed in *E. coli* Tuner strain (Novagen) co-expressing the RIL Codon Plus plasmid. Transformed cells were grown at 37°C in 2xYT media containing 100 μg/ml ampicillin and 34 μg/ml chloramphenicol until they reach OD 0.6. Protein expression was then induced with 200 μM IPTG over a 16 h period at 16° C. The cells were harvested, frozen and resuspended with buffer A (50mM Phosphate buffer pH 8, 400mM NaCl, 5% glycerol, 5mM β-mercaproethanol, 0.5mM EDTA, 2mM PMSF and protease inhibitor cocktail from Roche) and lysed using a microfluidizer followed by two cycles of centrifugation (12000 x g 20 min). Supernatant was then filtered with a 45 μm filter and loaded onto a pre-equilibrated Ni-chelate column (50 mM Phosphate buffer pH 8, 400 mM NaCl, 5% glycerol, 5 mM β-mercaproethanol). The column was washed with buffer A supplemented with 25 mM Imidazole until a stable baseline was achieved. Elution was then carried out in one step of 250 mM Imidazole, after which protein-containing fractions were pooled, supplemented with 5 mM EDTA, diluted 6 times with 50 mM Tris-HCl pH 8.2, 5 mM EDTA, 1 mM DTT and loaded onto pre-equilibrated Ion Exchange column (Capto HiRes Q 10/100 column, Cytiva). The protein was eluted in a range of 100-350 mM NaCl, 25 mM Tris-HCl pH 8.2. The protein was finally flash-frozen and store at -80°C for further biochemical assays.

CyclinB1-NT was ligated into the pGEX-4T-1 plasmid using BamHI and EcoRI sites, to generate GST fusion vector pGEX–GST-CyclinB1-NT. The plasmid was then transformed into competent *E. coli* BL21 (DE3) cells, and the transformed cells were grown in 1 l LB medium with 100 μg ampicillin/ml at 200 rpm at 37°C. Overnight cultures were diluted 1:100 into fresh LB medium. When the cell density reached about 0.6 OD600, the expression of fusion proteins was initiated by adding 0.5 mM IPTG. After 16 h induction at 200 rpm at 16°C, the cells were collected by centrifugation at 7000g at 4°C for 20 mins. The cell pellets were washed

and resuspended in 50 ml of ice-cold phosphate-buffered saline. The cells were broken by brief pulses of sonication on ice and a final concentration of 0.5 mM PMSF and 1% triton X-100 was added. The cell debris was removed by centrifugation at 12,000g for 20 mins at 4°C. The presence of the fusion protein in the supernatant was analyzed by 12% SDS–PAGE. The supernatant containing the fusion protein GST-CyclinB1-NT was loaded onto a Glutathione Sepharose (GST-Trap) affinity chromatography column equilibrated with PBS to purify the GST fusion protein. Then, the column was washed with 10 bed volumes of ice-cold PBS to remove contaminating proteins. The fusion protein was eluted with 10 bed volumes of freshly made 20 mM reduced glutathione elution buffer (0.308 g of reduced glutathione dissolved in 50 ml of 50 mM Tris–HCl, pH 8.0). The fusion protein containing fractions were pooled and dialyzed overnight in dialysis buffer (2 liters) in 10 molecular weight cut-off snake skin dialysis bag (50mM Tris pH 8.0, 150 mM NaCl, 1 mM DTT). After dialysis, the fusion protein was concentrated using Centricon™Microconcentrators. Protein concentration was determined by the method of Bradford using BSA as a protein standard.

In vitro degradation assay with purified proteasomes

Proteasomes were purified and tested for their activity using the in-gel proteasome assay as described previously.[33] *In vitro* degradation assays were done in total volume of 20 μl reaction mixture that includes purified 20 nM of human 26S or 20S proteasomes and the substrates, His-tagged GFP-ETV1 or FBXO6 in a molar ratio of 1:150. The percentage of substrate cleavage was compared with purified GST-Cyclin-B1-NT and β-casein (Sigma Chemicals, St Louis, MO, USA) (used as positive controls) and purified His-GFP (used as a negative control). The 26S proteasome assay buffer contained 25 mM Tris (pH 7.4), 10 mM MgCl2, 10% glycerol, 1 mM ATP, and 1 mM DTT. The 20S proteasome assay buffer contained 25 mM Tris (pH 7.4), 150 mM NaCl, 10% glycerol without MgCl2 and ATP. All degradation reactions were carried out at 37°C for up to 9 h and were terminated by adding SDS-loading dye and results were analyzed by 12-15% SDS-PAGE followed by immunoblotting and Coomassie staining. All *in vitro* assays were executed and tested for their reproducibility at least three times independently.

Rescue experiment with UBQLN1 cDNA

HEK293T Ubiquilins triple KO cells expressing GFP-fused full-length ORFs, ABCC5, REC8 and LRRN4CL were transduced with lentiviruses carrying HA-UBQLN1 wild-type or deletion mutants. It should be noted that the lentiviral plasmids encoding HA-UBQLN1 variants also contain an IRES BFP cassette to enable gating by flow cytometry equal expression of the constructs based on the BFP levels. 48 h post transduction, half of each sample was analyzed by flow cytometry to monitor the stability of GFP-fused ORFs and the rest was used for preparation of cell lysate used in western blot to examine expression of the constructs.

Microscopy

U2OS cells grown on cover slips were fixed for 15 min with 4% formaldehyde, followed by permeabilizing and blocking with 3% BSA, 0.5% Triton in PBS. Following 3 washes with PBS-T, DAPI staining (Sigma-Aldrich, #D9542) was added for 1 min. Finally, cover slips were mounted onto slides using mounting media (Sigma-Aldrich, F6182) prior to imaging. Cells were imaged with Leica Stellaris 5 confocal microscope using LASX software, and a 63× oil lens /1.4 N.A. UPlanSApo objective (Olympus).

Generation of GPS-peptides libraries

Generation and cloning of the original GPS-C23mers was described before.[25] Briefly, protein-coding sequences for all human proteins were downloaded from the RefSeq database and the terminal 23 amino acids of each selected for oligonucleotide design (27,030 sequences in total). Protein sequences were encoded as DNA bases using random codons, common 15 bp flanking primer sequences were added at each end and the oligonucleotide library was synthesized by Agilent. The pool of oligonucleotides was amplified by PCR (Q5 Hot Start High-Fidelity DNA Polymerase, NEB) and inserted into pHAGE-GPS3.0-DEST via Gateway BP and LR recombination reactions. Cloned libraries were transformed into ElectroMAX DH10β *E. coli* to achieve high coverage. After 1 h recovery in 1 mL SOC at 37°C, cells were spread on 15 cm LB + 100 μg/mL ampicilin plates. The following morning, cells were scraped and midiprepped to harvest the vector libraries. At least 100-fold representation of the library was maintained at each step.

GPS libraries for scanning mutagenesis were generated in an identical manner. Three mutagenesis libraries were generated: single substitution, triple substitution, and triple deletions.

For the single and triple substitutions libraries the following substitution ''code'' was used:

'A'>'R', 'G'>'R', 'V'>'R', 'L'>'R', 'I'>'R', #small nonpolar to big and charged (R) ##except at -3 where 'H' substitution is used.

'M'>'S', 'W'>'S', 'F'>'S', 'P'>'S', #large nonpolar to small polar (S).

'S'>'R', 'T'>'R', 'C'>'R', #small polar to big and charged (R) ##except at -3 where 'H' substitution is used.

'Y'>'A', 'N'>'A', 'Q'>'A', #large polar to small nonpolar (A) ##except at -1/-2 where 'S' substitution is used.

'D'>'R', 'E'>'R', #acidic to basic (R) ##except at -3 where 'H' substitution is used.

'K'>'A', 'R'>'A', 'H'>'A' #basic to small non-polar (A) ##except at -1/-2 where 'S' substitution is used.

This ''code'' was used to create maximum disruption to any potential degron, but only by replacing with amino acids that we found previously to have a neutral effect on stability (hence using R, S and A). In addition, we tried to avoid creating new C-terminal degrons, so a mutation to e.g. R-3 was swapped to H-3, and A-1/-2 was swapped to S-1/-2. In singles mutagenesis library, single mutations were used as above, whereas in triples mutagenesis library, each set of three consecutive amino acids were mutated as above, and triple deletions library, each set of three consecutive amino acids deleted (giving a set of mutant peptides that were each three amino

acids shorter). A recoded replicate of the wild-type peptide in each case was included as well. Figures 3D and S3A represent heatmaps comparing ΔPSI of mutant versus wild-type peptides. In triples mutagenesis experiments, for each amino acid shown, the average ΔPSI of the three consecutive position that contain the specific mutated amino acid is presented in the heatmaps.

Saturation mutagenesis library was generated in an identical manner. For each amino acid in the peptide sequence, a set of mutant sequences were generated in which the residue was mutated in turn to all of the other 19 possible amino acids. For each peptide, 9 reference sequences were also synthesized, in which the same wild-type amino acid sequence was encoded by different nucleotide sequences. Mutagenesis libraries were cloned into the pHAGE-GPS3.0-DEST, screened and sequenced as explained before.

GPS screens

GPS plasmid libraries were packaged into lentiviral particles which were used to transduce HEK293T cells at a multiplicity of infection of ~0.2 (achieving approximately 20% DsRed$^+$ cells) and at sufficient scale to achieve ~500-fold coverage of the library. Puromycin (1.5 μg/ml) was added two days post-transduction to eliminate untransduced cells. Surviving cells were pooled, expanded, and then partitioned by FACS into bins 7 days post-transduction based on the GFP/dsRed ratio. Genomic DNA was extracted from each of the pools separately (Gentra Puregene Cell Kit, Qiagen) and the fusion peptides or barcodes (ORF screen) amplified by PCR (Q5 Hot Start Polymerase, NEB) using a forward primer annealing to end of GFP and reverse primer annealing to the pHAGE vector; sufficient reactions were performed to amplify a total mass of DNA equivalent to the mass of genomic DNA from cells representing 500-fold coverage of the library. All PCR products were pooled, and one-tenth of the mix was purified using a spin column (Qiagen PCR purification kit). Finally, 200 ng of the purified PCR product was used as the template for a second PCR reaction using primers to add the Illumina P5 sequence and a 7 bp 'stagger' region to the 5' end, and Illumina indexes and P7 sequence at the 3' end. Samples to be multiplexed were then pooled, purified on an agarose gel (QIAEXII Gel Extraction Kit, Qiagen) and sequenced on an Illumina NextSeq instrument.

QUANTIFICATION AND STATISTICAL ANALYSIS

Analysis of GPS-C23mer screen

Raw Illumina reads derived from each GPS bin were first trimmed of constant sequences derived from the GPS vector backbone using Cutadapt.[76] Resulting 72 nucleotide reads were mapped to the reference input library using Bowtie 2[77] and count tables were generated from reads that aligned perfectly to the reference sequence. Following correction for sequencing depth, the protein stability index (PSI) metric was calculated for each GFP-peptide fusion. The PSI score is given by the sum of multiplying the proportion of reads in each bin by the bin number (1-6 in this case), thus yielding a stability score between 1 (maximally unstable) and 6 (maximally unstable):

$$\mathrm{PSI} = \sum_{i=1}^{6} Ri * i$$

(where i represents the number of the bin and R_i represents the proportion of Illumina reads present for a peptide in that given bin i). Read counts and associated stability score for each GFP-peptide fusion are detailed in Table S1.

A ΔPSI score was generated for each GFP-peptide fusion reflecting the difference in raw PSI scores between untreated sample and MLN7243 or bortezomib treatment. GFP-peptide fusions were defined as *UbInPD* substrates if they were stabilized $\geq$0.5 PSI units with bortezomib ($\Delta PSI_{bort} \geq 0.5$) but showed no or minor stability change, <0.2 PSI units, in response to MLN7243 ($\Delta PSI_{MLN} < 0.2$). We considered ubiquitin-dependent proteasome-dependent substrates as those with $\Delta PSI_{bort} \geq 0.5$ and $\Delta PSI_{MLN} \geq 0.2$.

Histograms presented in Figures 2A, S1C, S1D, S2A, S5C, S5D, S6D, and S6E show the proportion of corrected count reads in each one of the bins for the indicated GFP-fusions. Stabilization by the indicated inhibitors is indicated by a sharp peak to the right side of each panel.

Analysis of GPS-ORFeome screen

Illumina reads were trimmed of constant regions derived from the backbone of the GPS expression vector using Cutadapt. The number of occurrences of each of the 24 nucleotide barcode sequences that remained was then quantified using Bowtie 2. In the majority of cases barcodes could be uniquely assigned to individual ORFs; however, in cases where a barcode could not distinguish between multiple isoforms of the same gene (indicated by a lower case 'ioh' identifier in Table S3), read counts were assigned to all isoforms of that gene. After correcting for sequencing depth, the stability of each individual barcoded ORF was using the PSI metric, yielding a stability score between 1 (maximally unstable) and 4 (maximally stable).

A ΔPSI score was generated for each barcode reflecting the difference in raw PSI scores between untreated sample and MLN7243 or bortezomib treatment. Then, average of ΔPSI score of all barcodes of a single ORF were calculated to obtain an ORF ΔPSI. GFP-ORF fusions were defined as *UbInPD* substrates if they showed $\Delta PSI_{bort} \geq 0.3$ and $\Delta PSI_{MLN} \leq 0$. In addition, histograms showing the distributions of reads of each of the individual barcodes across all treatments were plotted. Those were manually reviewed to filter outs those whose barcodes performance is not consistent.

Analysis of mutagenesis GPS-C23mer screens

The heatmaps displayed in Figures 3D, 3E, and S3A illustrate the difference between the PSI for each individual mutant peptide and the average of wild type peptides; the darker the red color, the greater the stabilizing effect of the mutation.

Analysis of Disorder tendency

Disorder tendency was calculated using the disorder tendency prediction tool IUPred2A.[81] The tool was run locally with prediction type-long on full-length ORFs comparing library to ubiquitin-independent substrates. Each ORF in the library was assigned a fraction disorder score based on the fraction of resides with disorder tendency of >0.5. Comparing the library to ubiquitin-independent substrates revealed no significant difference (p=0.6767, t test). Data is presented in Table S5.

Statistical analysis of the distribution of PSI scores for all *UbInPD* peptides harboring specific C-terminal motifs

The significance of the statistics for the indicated C-terminal motifs was calculated using t-test and is presented in the table below as well as in Figure 3B.

	p-value		
Motif	Bortezomib vs. untreated	Bortezomib vs. MLN7243	MLN7243 vs. untreated
Ala-end	$2.147803e^{-121}$	$7.794270e^{-171}$	$1.488184e^{-16}$
Cys-end	$1.373704e^{-69}$	$1.190345e^{-97}$	$1.672087e^{-09}$
Val-end	$1.608453e^{-180}$	$7.771615e^{-258}$	$1.471684e^{-25}$

Quantification of *in vitro* degradation assays

ImageJ software was used for quantification and statistics of protein bands from scanned gels/blots of the degradation assays. Graphpad Prism V9 software was used for plotting the quantified data in graphs presented in Figures 5B, 5D, 5F, S4D, and S4F.